Acta Pharmaceutica Sinica B 2024;14(3):1166−1186

Chinese Pharmaceutical Association
Institute of Materia Medica, Chinese Academy of Medical Sciences

Acta Pharmaceutica Sinica B

www.elsevier.com/locate/apsb
www.sciencedirect.com

ORIGINAL ARTICLE

Extracellular vesicles from human urine-derived stem cells delay aging through the transfer of PLAU and TIMP1

Shanshan Rao[a,b,†], Zehui He[a,b,†], Zun Wang[a,b,c], Hao Yin[a,b], Xiongke Hu[a,b,d], Yijuan Tan[a,b], Tengfei Wan[a,b], Hao Zhu[a,b], Yi Luo[a,b], Xin Wang[a,b], Hongming Li[a,b], Zhenxing Wang[a,b], Xinyue Hu[e], Chungu Hong[a,b], Yiyi Wang[a,b], Mingjie Luo[c,f], Wei Du[a,g], Yuxuan Qian[a,b], Siyuan Tang[c,*], Hui Xie[a,b,h,*], Chunyuan Chen[a,b,*]

[a]*Department of Orthopedics, Movement System Injury and Repair Research Center, Xiangya Hospital, Central South University, Changsha 410008, China*
[b]*Hunan Key Laboratory of Angmedicine, Changsha 410008, China*
[c]*Xiangya School of Nursing, Central South University, Changsha 410013, China*
[d]*Department of Pediatric Orthopedics, Hunan Children's Hospital, University of South China, Changsha 410007, China*
[e]*Department of Respiratory Medicine, Xiangya Hospital, Central South University, Changsha 410008, China*
[f]*School of Nursing, Xinjiang Medical University, Urumqi, Xinjiang 830000, China*
[g]*Department of Rehabilitation, Xiangya Hospital, Central South University, Changsha 410008, China*
[h]*National Clinical Research Center for Geriatric Disorders, Xiangya Hospital, Central South University, Changsha 410008, China*

Received 17 September 2023; received in revised form 21 November 2023; accepted 22 November 2023

KEY WORDS

Extracellular vesicles;
Urine-derived stem cells;
Cellular senescence;
Anti-aging;
PLAU;

Abstract Aging increases the risks of various diseases and the vulnerability to death. Cellular senescence is a hallmark of aging that contributes greatly to aging and aging-related diseases. This study demonstrates that extracellular vesicles from human urine-derived stem cells (USC-EVs) efficiently inhibit cellular senescence *in vitro* and *in vivo*. The intravenous injection of USC-EVs improves cognitive function, increases physical fitness and bone quality, and alleviates aging-related structural changes in different organs of senescence-accelerated mice and natural aging mice. The anti-aging effects of

*Corresponding authors.
E-mail addresses: chency19@csu.edu.cn (Chunyuan Chen), huixie@csu.edu.cn (Hui Xie), sytang263@csu.edu.cn (Siyuan Tang).
[†]These authors made equal contributions to this work.
Peer review under the responsibility of Chinese Pharmaceutical Association and Institute of Materia Medica, Chinese Academy of Medical Sciences.

https://doi.org/10.1016/j.apsb.2023.12.009

TIMP1;
Senescence-accelerated mice;
Natural aging mice

USC-EVs are not obviously affected by the USC donors' ages, genders, or health status. Proteomic analysis reveals that USC-EVs are enriched with plasminogen activator urokinase (PLAU) and tissue inhibitor of metalloproteinases 1 (TIMP1). These two proteins contribute importantly to the anti-senescent effects of USC-EVs associated with the inhibition of matrix metalloproteinases, cyclin-dependent kinase inhibitor 2A ($P16^{INK4a}$), and cyclin-dependent kinase inhibitor 1A ($P21^{cip1}$). These findings suggest a great potential of autologous USC-EVs as a promising anti-aging agent by transferring PLAU and TIMP1 proteins.

1. Introduction

Aging process is accompanied with the increase of skin wrinkles, the decline of learning and memory ability, the loss of bone/muscle mass and strength, and the ever-increasing susceptibility to various diseases and even to death[1–4]. Cellular senescence and stem cell exhaustion are hallmarks of aging[4]. Senescent cells enter a stable state of cell cycle arrest and release abundant pro-inflammatory cytokines and matrix metalloproteinases (MMPs), which are termed "senescence-associated secretory phenotype (SASP)" factors and can aggravate aging[4–6]. The exhaustion of stem cells is a notable characteristic of aging and refers to a reduction in stem cell number and function associated with stem cell senescence[7]. Stem cell exhaustion leads to the decline of tissue regenerative capacity and the failure of multiple organs[4,8]. This opens the possibility of designing strategies for suppressing cellular senescence and increasing stem cell abundance and function to attenuate aging and age-related diseases.

Transplantation of young and healthy stem cells has been shown to increase health and lifespan in aged mice[9]. A study by Lavasani et al.[10] has reported that the intraperitoneal injection of muscle stem/progenitor cells from young mice can extend healthspan and lifespan in progeroid mice. Interestingly, the transplanted cells are not detected in many rejuvenated tissues[10], suggesting that their anti-aging effects are mainly mediated by activating endogenous cells in the host through the paracrine factors. Secretion of extracellular vesicles (EVs) is a part of normal physiology in both prokaryotes and eukaryotes[11,12]. EVs are selectively enriched with various molecules such as proteins and nucleic acids from their parent cells and serve as a key mediator of cell paracrine action by transferring these molecules to their recipient cells[13–16]. Stem cells-derived EVs have become an attractive option for therapeutic uses because these nanoparticles have fewer safety concerns and are easy to store, transport, and use compared with stem cells themselves. Recent studies have reported that EVs from embryonic stem cells[17,18], induced pluripotent stem cells[19], adipose stem cells[20,21], hypothalamic stem/progenitor cells[22], and umbilical cord- or umbilical cord blood-derived MSCs[23,24] can alleviate aging-related phenotypes in aged mice, indicating the promising potential of EVs as an anti-aging agent. Nevertheless, the use of these stem cells as the "factory" to harvest EV are limited by many problems, such as the ethical issue for cell use, the lack of enough source to obtain cells, or/and the requirement of fast, convenient, and invasive procedures for cell isolation.

As compared with stem cells from other sources, urine-derived stem cells (USCs) can be collected by a low-cost, simple, and safe method without ethical concerns. We have previously demonstrated that the local injection of USC-derived EVs (USC-EVs) can accelerate wound repair in diabetic mice by enhancing angiogenesis[16]. We have also found that the intravenous injection of USC-EVs can reduce bone loss and enhance bone strength in osteoporotic mice[14]. Moreover, these nanovesicles can exert protective effects against glucocorticoid-induced osteonecrosis by promoting angiogenesis, and suppress cell apoptosis after systemic administration[15]. In our previous study, we obtained proteomic data regarding the differentially expressed proteins between USC-EVs and USCs[16]. In this study, we further analyzed these data and found that a class of USC-EVs-enriched proteins have been previously shown to possess anti-aging function, such as tissue inhibitor of metalloproteinases 1 (TIMP1)[25], plasminogen activator urokinase (PLAU)[26], insulin-like growth factor binding protein 5[27], senescence marker protein-30[28], and connective tissue growth factor[29]. Thus, we hypothesized that USC-EVs might be capable of rejuvenating old organs from aging *via* transferring of anti-aging proteins.

Here, we tested the effects of USC-EVs on cellular senescence *in vitro* and on the aging-related phenotypes in different organs of both senescence-accelerated mice and natural aging mice. Then, we compared the anti-aging function of USC-EVs from donors with different ages, genders, and health conditions. Furthermore, we screened the candidate anti-senescent proteins in USC-EVs and confirmed their contributions to the USC-EVs-induced anti-aging effects *in vitro* and *in vivo*.

2. Materials and methods

2.1. Isolation and characterization of USCs and USC-EVs

The collection of human urine for harvesting USCs and the use of USC-EVs for experiments were approved by the USC donors with written informed consents. USCs were harvested from urine samples of two women with postmenopausal osteoporosis and seven healthy people of different ages and genders as previously described[14]. The procedures for USCs isolation and culture were detailed in our earlier study[16]. The identification of USCs and USC-EVs was described in the Supporting Material.

2.2. Cell culture and treatments

The sources and culture conditions of CAD, HL-1, C2C12, and BMSCs were detailed in Supporting Information. To induce senescence and neurite growth of CAD, the culture medium of

these cells was replaced with fresh serum-free DMEM/F-12 and the cells were incubated for 3 days. Then, the medium was replaced with fresh serum-free DMEM/F-12 containing USC-EVs, EVs from control short hairpin RNAs (shCon)-treated USCs (USC^{shCon}-EVs), EVs from shPLAU-transfected USCs (USC^{shPLAU}-EVs), EVs from shTIMP1-transfected USCs ($USC^{shTIMP1}$-EVs), or an equal volume of vehicle (PBS). Cells in the un-induced group were maintained in DMEM/F-12 added with 10% FBS and an equal volume of phosphate buffered saline (PBS: vehicle of USC-EVs). After treatment with USC-EVs or vehicle for 24 h, the cells were washed, fixed, and stained for SA-β-Gal. To test the effects of USC-EVs on hydrogen peroxide-induced cell senescence and the roles of PLAU and TIMP1 in this process, the above cells were cultured in complete medium with hydrogen peroxide (Sinopharm Chemical Reagent, Shanghai, China) + USC-EVs from different donors, hydrogen peroxide + USC^{shCon}-EVs, hydrogen peroxide + USC^{shPLAU}-EVs, hydrogen peroxide + $USC^{shTIMP1}$-EVs, or hydrogen peroxide + vehicle (control) for 24 h. Then, the cells were processed for SA-β-Gal staining and annexin V-FITC/PI staining followed by flow cytometry. Hydrogen peroxide and EVs were used at the dose of 100 μmol/L and 100 μg/mL, respectively. To evaluate the effects of USC-EVs on hydrogen peroxide-induced cytotoxicity, the above cells were treated with hydrogen peroxide + USC-EVs or hydrogen peroxide + vehicle for 24 h and then subjected to CCK-8 assay. To investigate the involvement of MMPs and PI3K−Akt signaling in the USC-EVs- and their enriched proteins PLAU- and TIMP1-induced anti-senescent effects in HL-1, C2C12, and BMSCs, these cells were cultured in normal condition, or under senescent induction by hydrogen peroxide and treated with vehicle, PLAU (1 μg/mL; Nevoprotein, Suzhou, China), TIMP1 (1 μg/mL; Nevoprotein), USC^{shCon}-EVs, USC^{shPLAU}-EVs, or $USC^{shTIMP1}$-EVs. After 24 h, these cells were processed for Western blotting to detect the expression of MMP1, MMP12, phosphorylated-PI3K (P-PI3K), PI3K, $P16^{INK4a}$, and $P21^{Cip1}$. To assess whether the inhibition of MMPs or PI3K−Akt signaling could affect the anti-senescent effects of USC-EVs, PLAU, and TIMP1, the cells were treated with hydrogen peroxide with or without PLAU, TIMP1, ilomastat (10 nmol/L; Selleckchem, Houston, USA), wortmannin (10 nmol/L; MedChemExpress, NJ, USA), USC-EVs, ilomastat + USC-EVs, or wortmannin + USC-EVs. After 24 h of incubation, the cells were subjected to SA-β-Gal staining.

2.3. *EV uptake assay*

USCs were labeled with a lipophilic stain DiI (Thermo Fisher Scientific, Madison, Waltham, USA) as described in detail in our previous study[3]. The DiI-labeled USC-EVs were harvested from the culture supernatant by procedures described above and then added to the culture of CAD, HL-1, HSF, C2C12, and BMSCs. After incubation for 3 h, the treated cells were fixed with 4% paraformaldehyde (PFA) for 15 min, stained with DAPI (Vector Laboratories, Burlingame, USA), and detected under a fluorescence microscope (Carl Zeiss ApoTome, Jena, Germany).

2.4. *Proteomic analysis*

USCs from the above-mentioned 28-year-old healthy women and their EVs were collected for proteomic analysis, which was performed by Jingjie PTM BioLab (Hangzhou, China). The method for proteomic analysis, data processing, and bioinformatics analysis of the obtained data had been described in detail in our previously published study[16].

2.5. *Inhibition of PLAU and TIMP1*

The design and packaging lentivirus carrying *EGFP* gene and shCon or shRNAs targeting PLAU (#1, #2, and #3) or TIMP1 (#1, #2, and #3) were performed by Cyagen Biosciences (Guangzhou, China). To transfect USCs, these cells were seeded into 6-well culture plates and incubated in serum-free medium added with lentiviral particles (multiplicity of infection = 30) and polybrene (5 μg/mL; Cyagen). Twenty-four hours later, the medium was discarded and replaced by fresh complete medium. The efficiency of transfection was confirmed by detecting the percentage of cells expressing EGFP protein and qRT-PCR analysis of the expression of *Plau* and *Timp1* in USCs. The sequences of shRNAs were shown in the Supporting Information.

2.6. *qRT-PCR analysis*

USCs receiving different treatments were collected and subjected to total RNA extraction using the RNAiso plus reagent (Accurate Biology, Changsha, China). 500 ng RNA per sample was reverse transcribed to cDNA using all-in-one 1st-Strand cDNA Synthesis SuperMix (Novoprotein Scientific Inc., Suzhou, China). The product was subjected to qRT-PCR with SYBR Green qPCR Master Mix (Bimake, Houston, USA) on an FTC-3000 real-time PCR system (Funglyn Biotech, Canada). *GAPDH* was used for normalization. Primer sequences were detailed in Supporting Information.

2.7. *Western blotting*

The procedures for western blotting were detailed in the supplementary material. Anti-CD9 (1:500), anti-CD63 (1:500), anti-CD81 (1:500), and anti-PLAU (1:500) were purchased from Santa Cruz Biotechnology. Anti-TSG101 (1:1000) and anti-MMP1 (1:2000) were bought from ProteinTech (Chicago, USA). Anti-MMP12 (1:2000), anti-$P16^{INK4a}$ (1:3000), and anti-$P21^{Cip1}$ (1:3000) were purchased from Servicebio (Wuhan, China). Anti-TIMP1 (1:1000), anti-p-PI3K (1:1000), anti-PI3K (1:1000), and the secondary antibodies (1:5000) were obtained from Cell Signaling Technology (Danvers, USA).

2.8. *SA-β-gal staining*

After serum starvation or hydrogen peroxide treatment for 24 h, the cells were washed with PBS and treated with fixative provided by the commercial SA-β-gal staining kit (Yeasen Biotech, Shanghai, China) for 15 min. The cells were washed with PBS and then stained with SA-β-gal staining reagent. After incubation at 37 °C overnight in the absence of light, the SA-β-gal-stained cells (blue) were washed and observed under an optical microscope. The mean intensity of blue signals was assessed by Image-Pro Plus 6 software.

2.9. *CCK-8 assay*

Cells were plated into 96-well plates (5×10^3 cells for each well) and treated with vehicle (Un-induced group), hydrogen peroxide + vehicle (Control group), or hydrogen peroxide + USC-EVs for 24 h. Then, the cells were incubated in

fresh medium (100 μL for each well) with CCK-8 solution (10 μL for each well; 7Sea Biotech, Shanghai, China) for another 3 h. The blank group was just added with fresh medium containing CCK-8 without cells. The absorbance was read at 450 nm with the Thermo Scientific Varioskan LUX multimode microplate reader (Waltham, USA).

2.10. Apoptotic cell assay

Cells were incubated in serum-free condition and treated with vehicle, hydrogen peroxide, hydrogen peroxide + USC-EVs from different donors, hydrogen peroxide + USC^{shCon}-EVs, hydrogen peroxide + USC^{shPLAU}-EVs, hydrogen peroxide + $USC^{shTIMP1}$-EVs for 24 h. The cells were then washed with the binding buffer from the annexin V-FITC/PI staining kit (Yeasen Biotech), and stained with annexin V-FITC and PI solution for 15 min. After that, the cells were subjected to flow cytometry analysis.

2.11. Animal treatments

All experiments were conducted with the approval of Ethics Committee and animal experiments and followed the guidelines for the Care and Use of Laboratory Animals at Xiangya Hospital of Central South University. To test the distribution of USC-EVs, USC-EVs were labeled with 1,1-dioctadecyl-3,3,3,3-tetramethylindotricarbocyanine iodide (Santa Cruz) and intravenously injected into 16-month-old male aged C57BL/6J mice *via* the tail vein. Three hours later, the mice were killed. The heart, liver, spleen, lungs, kidneys, brain, femurs, and tibias were obtained and subjected to fluorescent imaging with a fluorescence molecular tomography *in vivo* imaging system (FMT-4000; PerkinElmer, USA). To test the anti-aging activity and the roles of PLAU and TIMP1 transporters of USC-EVs, SAMP8 mice or aged C57BL/6J mice (16-month-old male) were intravenously treated with USC-EVs from different donors, USC^{shCon}-EVs, USC^{shPLAU}-EVs, or $USC^{shTIMP1}$-EVs (100 μg EVs dissolved in 100 μL PBS) once a week. The mice were subjected to behavioral tests after treatment for 8 (SAMP mice) or 12 (C57BL/6J mice) weeks. Blood samples were collected for harvesting serum and the mice were killed to collect the tissues for further analyses.

2.12. MWM test

The maze (RD1101-MWM-M; Shanghai Mobiledatum Information Technology, Shanghai, China) is a black circular pool with a height of 50 cm and a diameter of 120 cm. The pool was filled with 24 ± 2 °C water (depth: 25 cm) and divided into four equal quadrants with prominent visual cues in each direction of every quadrant. A circular platform (height: 20−35 cm; diameter: 6 cm) was placed in the center of a quadrant and under 0.5 cm of the water surface. The mice receiving different treatments were trained every day for 4 days to assess spatial learning ability. In each training trial, the mice were placed into the water maze at one of the randomly selected locations in each quadrant and allowed to swim for a maximum of 60 s to find and climb onto the submerged platform. If the mice could not accomplish this task within 60 s, they were guided to find the platform and then stayed on it for 10 s. After training, the platform was submerged under 1 cm of the water surface and five consecutive days of testing trials were performed. The escape latency to the platform was recorded. To assess spatial memory ability, the platform was removed at 24 h after spatial learning test. The mice were placed into the water maze and allowed to search for the platform. The target quadrant occupancy (time spent in the target quadrant) and crossing times through the platform within 90 s were recorded. Each test was conducted three times with a 20 min interval in each session. The average data in the three repeated trials in a day were used for within-animal comparisons.

2.13. Grip strength test

To test the grip strength of the forelimbs, the mice in different groups were held by the tails and allowed to grasp the iron rod (diameter: 9 mm; length: 50 cm) on two mounting brackets (height: 40 cm) by their forepaws. Then, their tails were gently released so that the mice could hang on the rod. The timer was started and continued until the mice released the rod. After 24 h of training three times, four consecutive days of testing trials (three times a day) were conducted. The latency to fall (time spent on the rod) for each mouse was recorded.

2.14. Balance beam test

A horizontal wooden beam (0.9 cm × 0.9 cm × 50 cm) was supported by two platforms (height: 40 cm) and a dark box was installed at the end of the beam. To test motor coordination and balance, the mice in different groups were individually placed on the beam at the same location opposite to the dark box and allowed to run across the beam to the dark box. After training for 24 h, testing trials were performed three times a day for four consecutive days. The time spent on the balance beam was recorded and the speed to cross the beam was calculated.

2.15. Rotarod test

The motor function of mice was also assessed by rotarod test with a commercial rotarod (Unibiolab, Beijing, China; diameter: 3 cm). The mice in different groups were individually placed on the rotating rotarod at a gradually increasing speed (accelerated speed: 5 rpm) from a slow initial speed to 60 rpm. After 24 h of training three times, testing trials were performed for four consecutive days (three times a day) and the latency to fall (time spent on the rotarod) for each mouse was recorded.

2.16. Three-point bending test

The strength of the left femurs was examined using a Instron 3343 biomechanical testing machine (Instron, Canton, USA). The specimens were placed on two parallel supporting bars (distance between these two bars: 8 mm) and loaded at the middle position in vertical direction. The compression load was maintained at a constant test velocity of 5 mm/min until fracture happened. The ultimate load (N) of the femur was determined according to the load−displacement curves generated by the machine.

2.17. μCT analysis

To assess bone microstructures, the right femurs were fixed with 4% PFA for 48 h and analyzed by a vivaCT80 μCT scanner (SCANCO Medical AG, Bruettisellen, Switzerland; resolution 11.5 μm per pixel, 45 kV, 100 μA). Three softwares including NRecon, CTAn v1.11, and μCTVol v2.0 were used to reconstruct, analyze, and visualize trabecular and cortical bones in the distal femurs. The region of interest (ROI) for trabecular bone analysis

was the area between 0.6 mm and 1.2 mm proximal to the distal growth plate, while the region for cortical bone analysis was started from the midpoint of femoral shaft and extended distally for 5% of femoral length. Tb. BV/TV, Tb. Th, Tb. N, Tb. Sp, Ps. Pm, Es. Pm, and Ct. Th were measured.

2.18. Histological and immunohistochemical analyses

The left brain was fixed for 6 h in 4% PFA, washed with PBS, dehydrated in 30% sucrose (Macklin, Shanghai, China), and then embedded in OCT (Sakura Finetek, Torrance, USA). 10-μm-thick brain sections were made and placed overnight at −20 °C. The cryopreserved brain sections were recovered at room temperature for 15 min and incubated overnight at 37 °C with SA-β-gal staining solution (Yeasen Biotech). The right brain, muscle, heart, and skin tissues were fixed in 4% PFA for 48 h, dehydrated using graded ethanol, immersed in n-butanol, and then embedded in paraffin. The right femur was fixed with 4% PFA for two days and decalcified for one week in 0.5% EDTA before dehydration, transparency, and embedding. These tissues were sectioned into 5-μm-thick slices and subjected to histological analysis or immunohistochemistry (IHC) staining. For histological analysis, the muscle and skin sections were stained with hematoxylin and eosin (H&E) staining reagents and Masson's trichrome stain (Servicebio), respectively, in order to determine the size of muscle fiber, the extent of collagen deposition, and the thickness of dermal tissues. The bone tissue sections were stained with TUNEL staining kit from Elabsceience (Wuhan, China). All of the above tissues were subjected to IHC staining for $p16^{INK4a}$, $P21^{Cip1}$, or/and collagen XVII (COL17A1). Primary antibodies and secondary antibodies were purchased from AiFang biological (Changsha, Hunan) or Servicebio, respectively. The procedures for IHC staining were detailed in our earlier study[4]. The mean intensity of the positive signals was determined by Image-Pro Plus 6 software.

2.19. SASP factor analysis

Serum specimens were stored at −80 °C before analysis. To assess the serum concentrations of SASP factors (IL-1α, IL-1β, IL-6, and TNF-α), the specimens were thawed and subjected to enzyme-linked immunosorbent assay (ELISA) using the commercial kits from MultiSciences (Lianke) Biotech (Hangzhou, China).

2.20. Statistical analysis

All data (mean ± SD) were analyzed using GraphPad Prism 8 software. Differences between two groups were determined by unpaired, two-tailed Student's *t*-test. One- or two-way analysis of variance (ANOVA) with Bonferroni *post hoc* test was used for the comparisons between multiple groups. Statistical significance was concluded when $P < 0.05$.

3. Results

3.1. USC-EVs attenuate serum deprivation- or hydrogen peroxide-induced cellular senescence and apoptosis

Supporting Information Fig. S1 shows the identification results of USCs from a 28-year-old healthy woman. Consistent with the results of our previous studies[14–16], USCs showed a spindle-like morphology (Fig. S1A), possessed the differentiation capacities towards osteoblasts (Fig. S1B-i), adipocytes (Fig. S1B-ii), and chondrocytes (Fig. S1B-iii), and displayed a marker expression profile of MSCs (Fig. S1C). USC-EVs had a cup-like morphology (Fig. 1A) with diameters mainly ranging from 50 to 100 nm (Fig. 1B) and positive for the exosomal markers (CD9, CD63, CD81, and TSG101; Fig. 1C), indicating that these EVs are primarily exosomes, the most characteristic EVs.

To examine the effects of USC-EVs on cellular senescence, we first determined whether USC-EVs could be taken up by different cells, including mouse neuronal cell line CAD, mouse cardiomyocyte cell line HL-1, mouse myoblast cell line C2C12, human skin fibroblasts (HSF), and primary bone marrow-derived MSCs (BMSCs). Fig. 1D shows abundant red fluorescent signals in the perinuclear region of CAD, HL-1, HSF, C2C12, and BMSCs after incubation with the red lipophilic dye DiI-labeled USC-EVs for 3 h, indicating the uptake of USC-EVs by these cells. CAD cells is a neuronal cell line in which neuronal differentiation can be induced by removal of serum[30]. Once cultured in serum-free condition, CAD cells stop proliferating and extend long neurites[30]. Consistently, our result showed that CAD cells extended neurites of different lengths in response to serum deprivation, but most of the differentiated CAD cells became senescent in response to serum deprivation, as revealed by the senescence-associated β-galactosidase (SA-β-gal) staining images and the quantitative data of neurite length and mean intensity for SA-β-gal (Fig. 1E–G). USC-EVs did not only significantly enhance the length of neurites of the differentiated CAD cells, but also markedly reduced the extent of serum deprivation-induced CAD senescence (Fig. 1E–G), indicating that USC-EVs can promote neurite growth and inhibit cellular senescence. SA-β-gal staining revealed that USC-EVs were also able to remarkably suppress hydrogen peroxide-induced senescence of HL-1, HSF, C2C12, and BMSCs (Fig. 1H and I). Cell counting kit-8 (CCK-8) assay indicated that treatment with hydrogen peroxide for 24 h profoundly inhibited the survival/growth of CAD, HL-1, HSF, C2C12, and BMSCs, but the changes were significantly reversed by co-incubation with USC-EVs (Fig. 1J). Increased cellular apoptosis occurs with the aging of various organs[31,32]. We further evaluated the effects of USC-EVs on cellular apoptosis. As evidenced by Annexin V-FITC/Propidium Iodide (PI) apoptosis analysis with flow cytometry, treatment with USC-EVs profoundly reduced the hydrogen peroxide-induced increase of late apoptotic/dead (Annexin V-$FITC^+$/PI^+; Q2) and/or early apoptotic (Annexin V-$FITC^+$/PI^-; Q3) CAD, HL-1, and C2C12 (Fig. 1K and Supporting Information Fig. S2). These findings indicate that USC-EVs can protect against serum deprivation- or hydrogen peroxide-induced cellular senescence and apoptosis.

3.2. USC-EVs exert anti-aging effects in senescence-accelerated mice and natural aging mice

We first assessed the tissue distribution of USC-EVs in aged mice after intravenous administration. As shown by *ex vivo* fluorescent imaging, the DIR-labeled USC-EVs could be detected in all the tested tissues of aged C57BL/6J mice (16-month-old; male) after intravenous injection for 3 h, with higher levels of accumulation in the mouse liver, spleen, lung, kidneys, and bones (femurs and tibias) (Fig. 2A), indicating that USC-EVs can be transported to various tissues of the recipient mice.

We then assessed the anti-aging effects of USC-EVs in both SAMP8 and natural aging mice. Evidence has shown that 100 μg EVs per animal one time a week for 6–12 weeks can induce

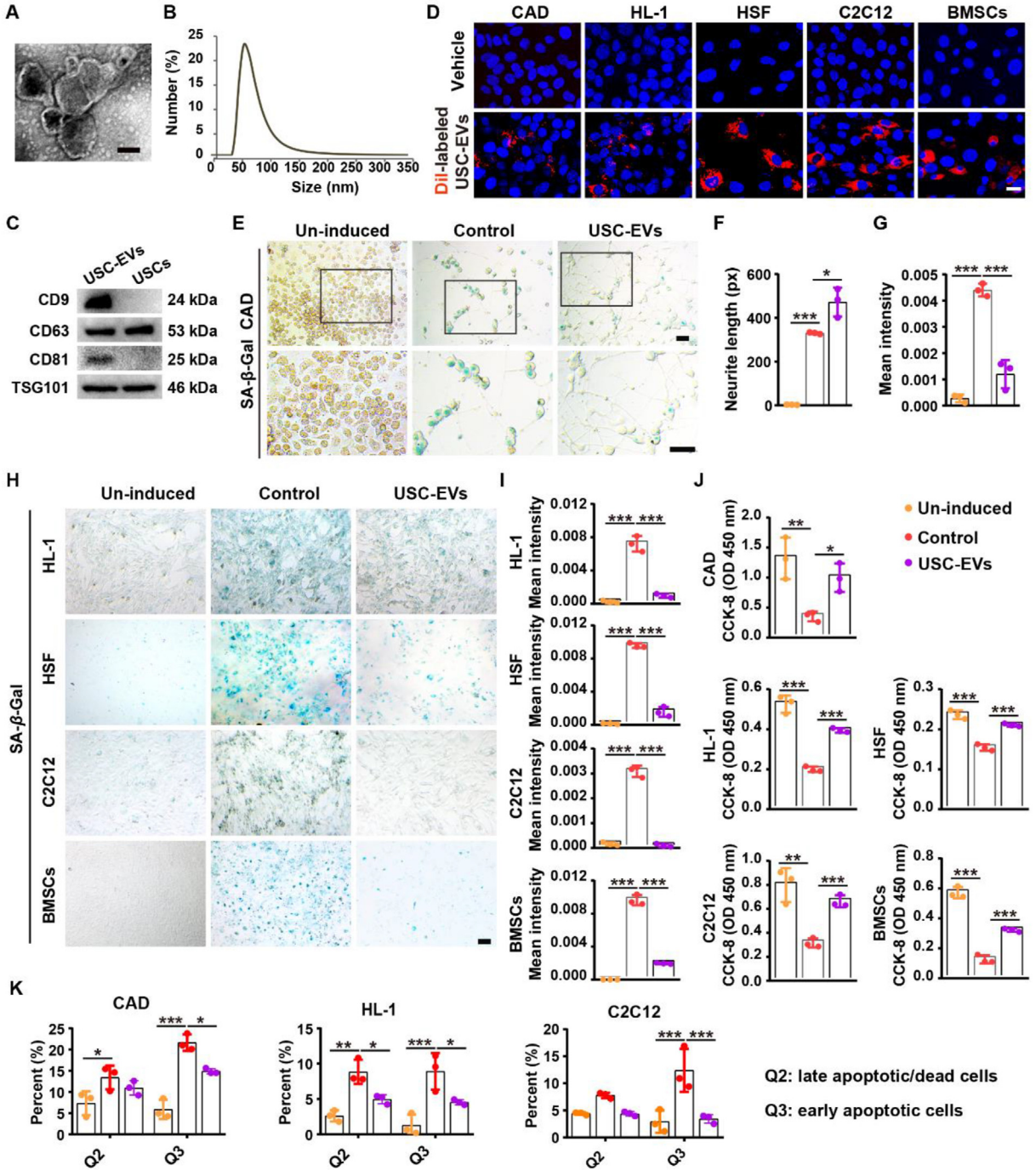

Figure 1 USC-EVs attenuate serum deprivation- or hydrogen peroxide-induced cellular senescence. (A)−(C) Assessments of morphology (A; Scale bar: 50 nm), diameter distribution (B), exosomal marker expression (C) by a transmission electron microscope, dynamic light scattering analysis, and Western blotting, respectively, in USC-EVs. (D) Uptake of the DiI (red)-labeled USC-EVs by different types of cells. Scale bar: 100 μm. (E) Senescence-associated β-galactosidase (SA-β-gal) staining images of CAD cells in complete culture medium (un-induced) or in serum-free condition receiving vehicle (control) or USC-EVs treatment. Scale bar: 50 μm. (F and G) Quantification of the mean intensity for the SA-β-gal-stained cells (F) and the length of neurites (G). $n = 3$ per group. (H) SA-β-gal staining images of different types of cells in normal culture medium (un-induced) or in hydrogen peroxide-containing medium added with vehicle (control) or USC-EVs. Scale bar: 50 μm. (I) Quantification of the mean intensity for the SA-β-gal-stained cells. $n = 3$ per group. (J) Cell counting kit-8 (CCK-8) analysis of the survival/growth of different types of cells in normal culture medium (un-induced) or in hydrogen peroxide-containing medium added with vehicle (control) or USC-EVs. $n = 3$ per group. (K) Cellular apoptosis was assessed by flow cytometry combined with annexin V-FITC/PI staining in hydrogen peroxide-induced senescent CAD, HL-1, and C2C12 with different treatments. The percentages of late apoptotic/dead cells (Q2) and early apoptotic cells (Q3) were measured. $n = 3$ per group. Data are shown as mean ± SD. $^{*}P < 0.05$, $^{**}P < 0.01$, $^{***}P < 0.001$.

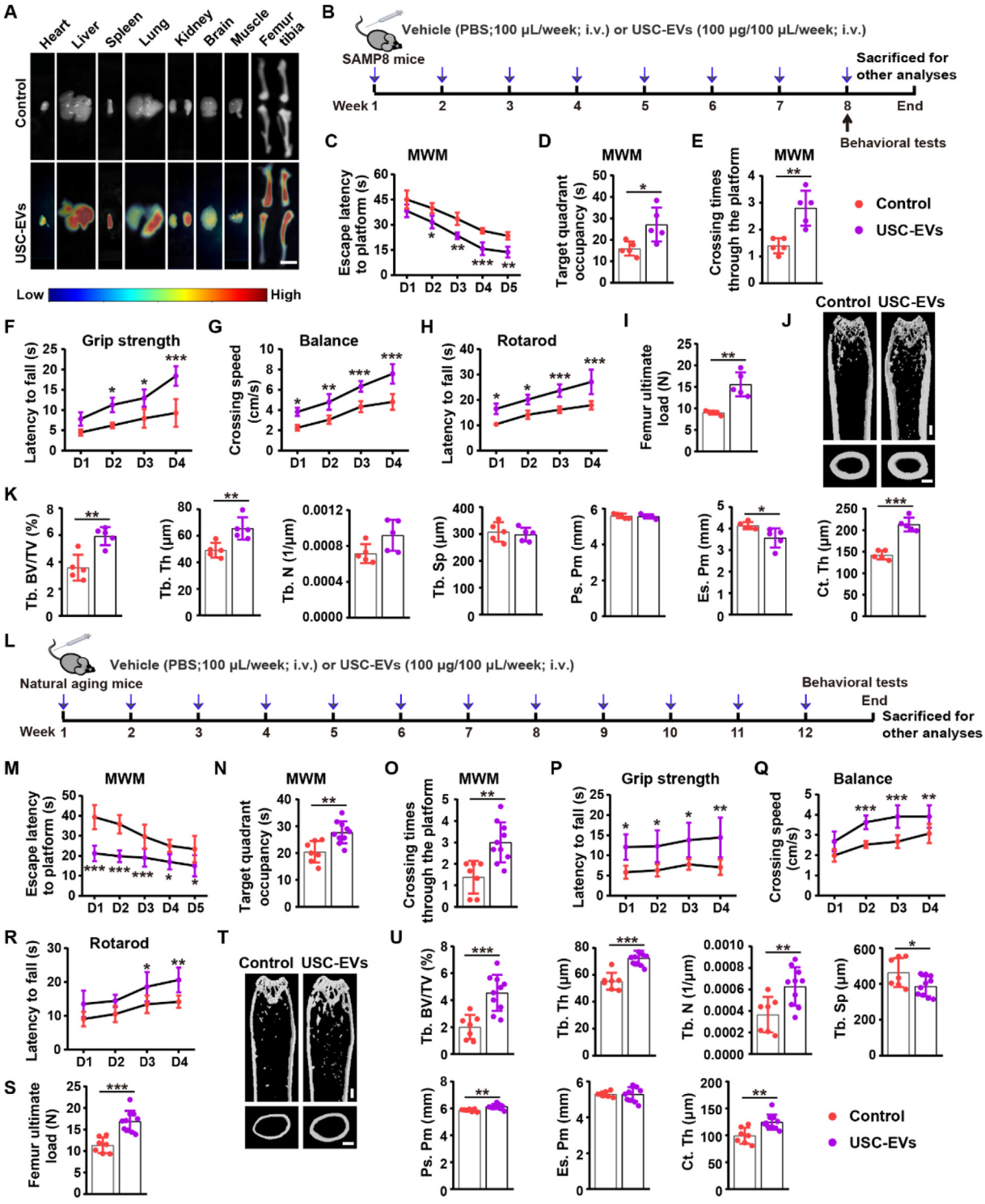

Figure 2 USC-EVs improve cognitive function, physical fitness, and bone quality in senescence-accelerated mice and natural aging mice. (A) *Ex vivo* fluorescent imaging of the DIR-labeled USC-EVs in different tissues after intravenous injection to mice for 3 h. Scale bar: 6 mm. (B) Schematic diagram for evaluating the anti-aging effects of USC-EVs by intravenous (i.v.) route in SAMP8 mice. (C)−(E) Spatial learning and memory abilities of the mice in (B) were examined by MWM test. The escape latency to platform (C), target quadrant occupancy (D), and crossing times through the platform (E) were recorded. $n = 5$ per group. (F) The muscle strength of the mice in (B) was assessed by grip strength test. The latency to fall from the rod was recorded. $n = 5$ per group. (G, H) The motor function of the mice in (B) were evaluated by balance beam test and rotarod test. The speed to cross the beam (G) and the latency fall from the rotarod (H) were measured. $n = 5$ per group. (I)−(K) Three-point bending test of the femur strength (I) and μCT-reconstructed femur images (j). Scale bar: 1 mm. $n = 5$ per group. (K) Quantification of bone microstructural parameters of femurs from mice in (B). $n = 5$ per group. (L) Schematic diagram for evaluating the anti-aging effects of USC-EVs in natural aging mice. (M)−(O) Morris water maze (MWM) test of the spatial learning and memory abilities of the mice in (L). $n = 7$−10 per

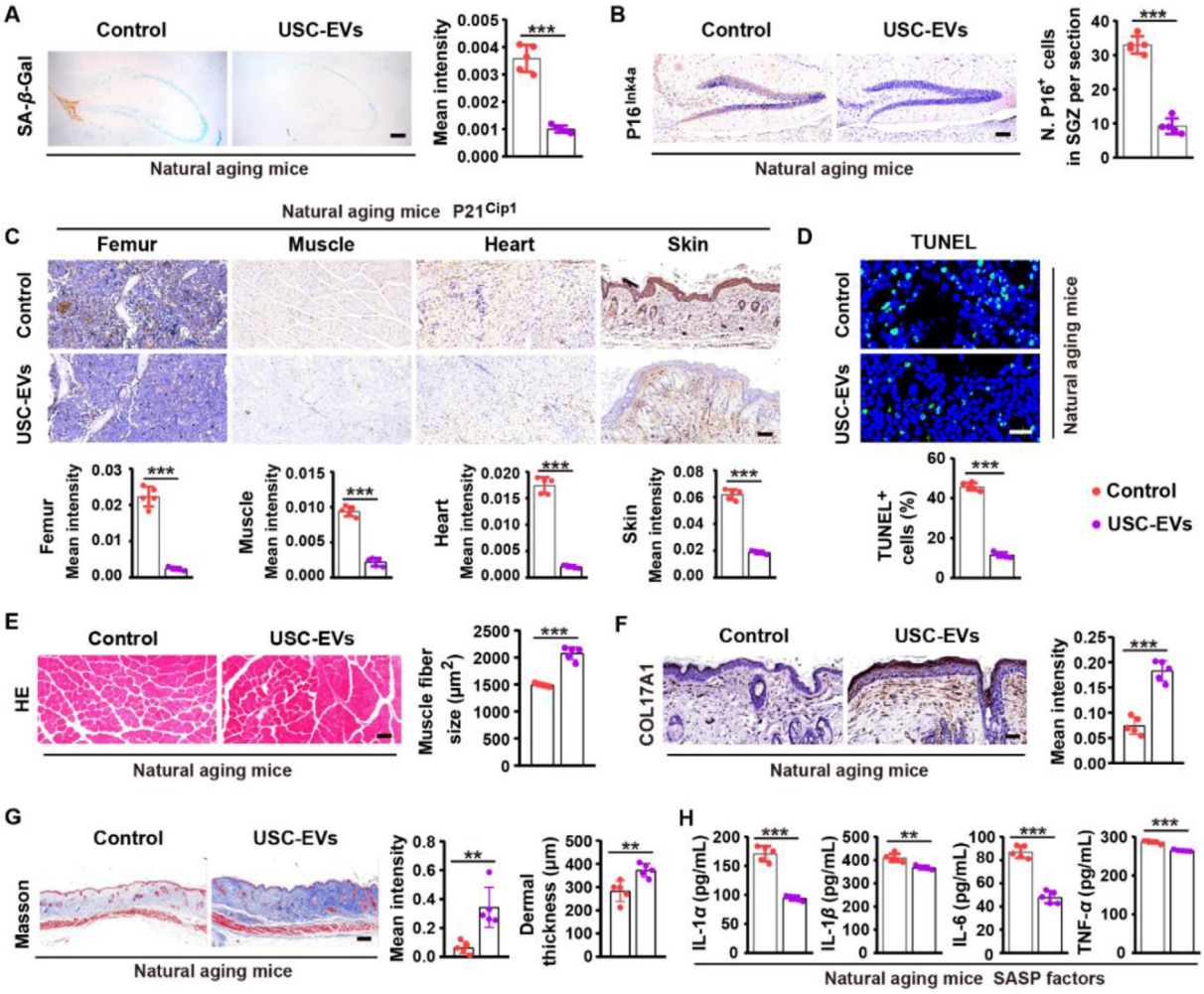

Figure 3 USC-EVs alleviate aging-related phenotypes in different organs of natural aging mice. (A) SA-β-gal staining images of the hippocampus and quantification of the mean staining intensity in the vehicle- or USC-EVs-treated natural aging mice. Scale bar: 500 μm. $n = 5$ per group. (B) Immunostaining images of cyclin-dependent kinase inhibitor 2A ($P16^{INK4a}$) in subgranular zone of the hippocampus and quantification of the mean staining intensity. Scale bar: 100 μm. $n = 5$ per group. (C) Immunostaining images of $P21^{Cip1}$ in different tissues and quantification of the mean staining intensity. Scale bar: 50 μm (for femurs) or 100 μm (for other tissues). $n = 5$ per group. (D) TUNEL staining images and quantification of apoptotic cell number in bone tissues. Scale bar: 20 μm. $n = 5$ per group. (E) H&E staining images of muscle tissues and quantification of the muscle fiber size. Scale bar: 100 μm. $n = 5$ per group. (F) Immunohistochemical staining for collagen type XVII (COL17A1) in skin tissues and quantification of the mean staining intensity. Scale bar: 50 μm. $n = 5$ per group. (G) Masson's trichrome staining for skin collagen fibers and quantification of the mean staining intensity and dermal thickness. Scale bar: 200 μm. $n = 5$ per group. (H) Serum concentrations of senescence-associated secretory phenotype (SASP) factors tested by ELISA. $n = 5$ per group. Data are shown as mean ± SD. $^{**}P < 0.01$, $^{***}P < 0.001$.

marked therapeutic benefits in animals[33–35]. We have found that the intravenous injection of USC-EVs (100 μg per mouse) weekly for 2 or 3 months induces significant bone-protective effects in osteoporotic mice[14]. Thus, USC-EV treatment (100 μg/mouse) was conducted once a week for 2 months in SAMP mice and for 3 months in natural aging mice through intravenous route. Fig. 2B shows the schematic diagram for evaluating the anti-aging effects of USC-EVs in SAMP8 mice. Morris water maze (MWM) test was conducted to assess the spatial learning and memory abilities of these treated mice. As shown in Fig. 2C–E, treatment with USC-EVs significantly reduced the escape latency, enhanced the target quadrant occupancy, and increased the crossing times through the platform in the MNM test, indicating that USC-EVs improve the cognitive function of SAMP8 mice. Grip strength test revealed that the USC-EVs-treated mice showed a longer latency to fall from the iron rod compared to the vehicle-treated control mice (Fig. 2F), revealing that USC-EVs enhance the muscle strength of SAMP8 mice. Balance beam test and rotarod

group. (P)–(R) Muscle strength and motor function assessments by grip strength test (P), balance beam test (Q), and rotarod test (R). $n = 7–10$ per group. (S) Three-point bending test of the femur strength. $n = 7–10$ per group. (T and U) μCT-reconstructed images of the femurs (T) and quantification of the bone microstructural parameters (U). Scale bar: 1 mm. $n = 7–10$ per group. Data are shown as mean ± SD. $^{*}P < 0.05$, $^{**}P < 0.01$, $^{***}P < 0.001$.

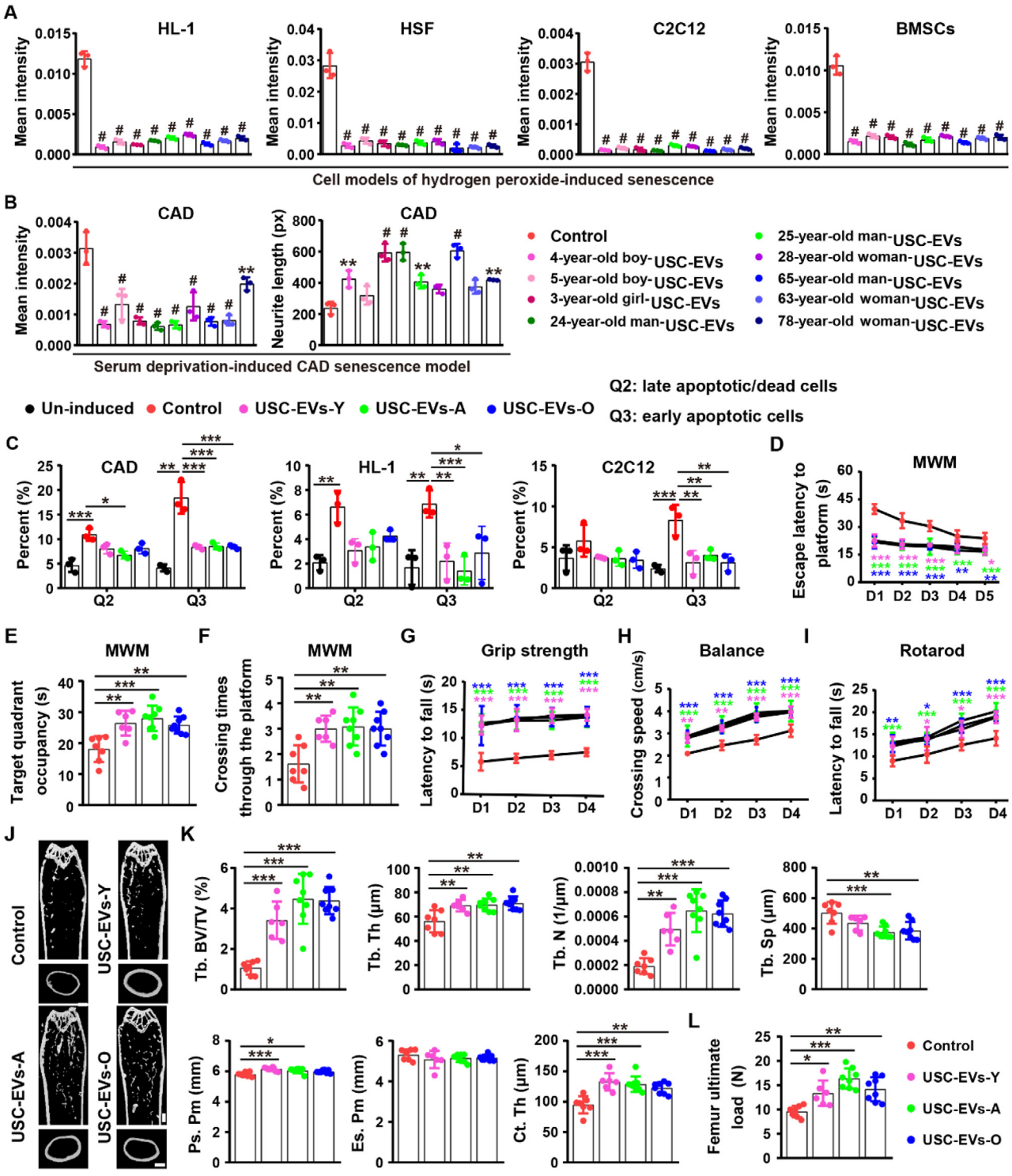

Figure 4 Multiple donor-derived USC-EVs inhibit cellular senescence, reduce cellular apoptosis, improve behavioral performance, and increase bone quality. (A) SA-β-gal staining was conducted in different types of cells treated with hydrogen peroxide + vehicle (control) or hydrogen peroxide + different donor-derived USC-EVs. The mean intensity of the SA-β-gal-stained cells was measured. $n = 3$ per group. (B) CAD cells treated with vehicle or different donor-derived USC-EVs in serum-free condition were subjected to SA-β-gal staining. The mean staining intensity and the length of neurites were quantified. $n = 3$ per group. (C) Apoptosis of different cell types receiving different treatments was measured by flow cytometry with annexin V-FITC/PI staining. The percents of late apoptotic/dead cells (Q2) and early apoptotic cells (Q3) were analyzed. $n = 3$ per group. (D)−(F) MWM test of the spatial learning and memory abilities of the natural aging mice treated with vehicle or different donor-derived USC-EVs. $n = 6$−8 per group. (G)−(I) Muscle strength and motor function assessments of the vehicle- or different donor-derived USC-EVs-treated natural aging mice by grip strength test (G), balance beam test (H), and rotarod test (I). $n = 6$−8 per group. (J, K) μCT-reconstructed images of the femurs (J) and quantification of the trabecular and cortical bone microstructural parameters (K) in

test showed that the USC-EVs-treated mice also exhibited a higher speed to cross the balance beam and a longer latency to fall from the rotarod compared with the control mice (Fig. 2G and H), indicating that USC-EVs can prevent the aging-induced decline of motor function including coordination, balance, and endurance of mice. Three-point bending test indicated a much higher femur bending strength of the USC-EVs-treated mice than that of the control mice (Fig. 2I). Microcomputed tomography (μCT) analysis revealed that USC-EVs markedly enhanced bone mass in SAMP8 mice, as indicated by the representative images of the trabecular and cortical bones of the femurs (Fig. 2J) and the significant changes of quantitative parameters including trabecular bone volume fraction (Tb. BV/TV), trabecular thickness (Tb. Th), endosteal perimeter (Es. Pm), and cortical thickness (*C*t. Th) (Fig. 2K). No obvious alterations were observed in the values of trabecular number (Tb. N), trabecular separation (Tb. Sp), and periosteal perimeter (Ps. Pm) (Fig. 2K).

We then tested the effects of USC-EVs on cognitive function, physical fitness, bone strength, and bone mass in 16-month-old natural aging mice after intravenous injection once a week for 12 weeks (Fig. 2L). Consistent with that observed in SAMP8 mice, MWM test showed that the administration of USC-EVs to natural aging mice caused a shorter escape latency to find the platform (Fig. 2M), a longer time in the target quadrant (Fig. 2N), and a higher frequency of crossing the platform (Fig. 2O). Other three behavioral tests including the grip strength test, the balance beam test, and the rotarod test revealed that USC-EVs also induced a longer latency to fall from the iron rod (Fig. 2P), a higher speed to cross the balance beam (Fig. 2Q), and a longer latency to fall from the rotarod in these mice (Fig. 2R). Three-point bending test and μCT analysis indicated that the USC-EVs-treated mice had much higher values of femur ultimate load, Tb. BV/TV, Tb. Th, Tb. N, Ps. Pm, and Ct. Th, as well as much lower value of Tb. Sp compared with the control mice (Fig. 2S−U). These findings demonstrate that USC-EVs can enhance spatial learning and memory abilities, muscle strength, motor function, bone mass, and bone strength of natural aging mice after intravenous administration.

We further detected the senescent phenotypes of different organs in both SAMP8 mice and natural aging mice. The hippocampus is a key brain area for spatial learning and memory. As shown in Supporting Information Fig. S3A and Fig. 3A, there were large numbers of senescent cells strong positive for SA-β-gal in the hippocampus of the vehicle-treated control mice, whereas the accumulation of hippocampal senescent cells was markedly attenuated in USC-EVs treatment group, indicating that USC-EVs effectively prevent hippocampus senescence. The subgranular zone (SGZ) of the dentate gyrus in the hippocampus is an important region for neurogenesis, which is closely associated with cognitive functions such as learning and memory[36]. Immunohistochemical staining for the senescence marker cyclin-dependent kinase inhibitor 2A ($P16^{INK4a}$) revealed that USC-EVs significantly reduced the number of $p16^{INK4a}$-positive senescent cells in SGZ region of SAMP mice (Fig. S3B) and natural aging mice (Fig. 3B), consistent with the benefits of USC-EVs on spatial learning and memory abilities of aged mice. Cyclin-dependent kinase inhibitor 1A ($P21^{Cip1}$) is another marker of senescence. As shown in Fig. S3C and Fig. 3C, immunohistochemical staining for $P21^{Cip1}$ showed that the senescent cells were accumulated in the femur, muscle, heart, and skin tissues of both SAMP8 mice and natural aging mice, but cellular senescence in these tissues was significantly mitigated in the USC-EVs-treated aged mice, as revealed by the much lower staining intensity for $P21^{Cip1}$ in these tissues of USC-EVs group than that of the control group. Terminal Deoxynucleotidyl Transferase mediated dUTP Nick-End Labeling (TUNEL) staining revealed that USC-EVs markedly reduced apoptotic cell numbers in the aged bone tissues (Fig. S3D and Fig. 3D). H&E staining indicated that USC-EVs could also increase the size of muscle fiber in these two types of aging mice (Fig. S3E and Fig. 3E), in accordance with the positive effect of USC-EVs on muscle strength. Collagen type XVII (COL17A1) plays an important role in the maintenance of skin homeostasis and "youthful", but its expression declines with age[37]. Immunostaining for COL17A1 indicated that USC-EVs treatment resulted in a remarkable increase of COL17A1 expression in both the epidermal and dermal tissues of the skin (Fig. S3F and Fig. 3F), indicating that USC-EVs can rejuvenate skin in aged mice. Masson's trichrome staining showed that USC-EVs not only increased collagen contents in skin tissues, but also enhanced the thickness of dermal tissues (Fig. S3G and Fig. 3G), which further demonstrate the anti-aging effects of USC-EVs on skin. SASP factor analysis by ELISA showed significant reductions of IL-1α, IL-1β, IL-6, and TNF-α in the USC-EVs-treated mice compared with the control mice (Fig. S3H and Fig. 3H). These results demonstrate that USC-EVs alleviate aging-related phenotypes in different organs and generate a "youthful" environment in SAMP8 mice and natural aging mice.

3.3. *Multiple donor-derived USC-EVs alleviate aging-associated phenotypes in vitro and in vivo*

Next, we obtained USCs from nine donors at different age phases, including three 3- to 5-year-old healthy children (two boys and one girl), three 24- to 28-year-old healthy adults (two men and one woman), and three 63- to 78-year-old people (a healthy man and two women with age- and menopause-related osteoporosis). Their derived USC-EVs were collected and the effects of these EVs on cellular senescence were compared. As revealed by SA-β-gal staining, USC-EVs from the above-described nine donors all could profoundly suppress hydrogen peroxide-induced senescence of HL-1, HSF, C2C12, and BMSCs (Fig. 4A). These donors-derived USC-EVs could also markedly decrease the extent of serum deprivation-induced CAD cellular senescence and increase the length of neurites formed by the differentiated CAD cells (Fig. 4B). No age-, gender-, or health condition (with or without osteoporosis)-related changes of the anti-senescent abilities were observed in these USC-EVs from different donors (Fig. 4A and B).

For each age phase (young, adult, and elderly), one donor-derived USC-EVs were selected and their anti-apoptotic ability was assessed. As indicated by flow cytometry analysis, USC-EVs from the young (Y: a 5-year-old healthy boy), adult (A: a 24-year-old healthy adult man), and old (O: a 63-year-old osteoporotic woman) donors could all notably reverse the hydrogen peroxide-induced increase of late apoptotic/dead (Annexin V-$FITC^+$/PI^+;

natural aging mice treated with vehicle or different donor-derived USC-EVs. Scale bar: 1 mm. $n = 6-8$ per group. (L) Three-point bending test of the femur strength in natural aging mice treated with vehicle or different donor-derived USC-EVs. $n = 6-8$ per group. Data are shown as mean ± SD. For panels (A, B): $^{**}P < 0.01$, $^{\#}P < 0.001$ *vs.* Control group. For other panels: $^{*}P < 0.05$, $^{**}P < 0.01$, $^{***}P < 0.001$.

Q2) and/or early apoptotic (Annexin V-FITC^{+}/PI^{-}; Q3) CAD, HL-1, and C2C12 cells (Supporting Information Fig. S4 and Fig. 4C). No significant changes of the anti-apoptotic effects were observed among these EVs (Fig. S4 and Fig. 4C).

The anti-aging effects of these USC-EVs were then evaluated in 16-month-old natural aging mice after intravenous injection once a week for 12 weeks. As revealed by MWM tests, treatment with either one of these donors-derived EVs could markedly reduce the escape latency (Fig. 4D), enhance the time in the target quadrant (Fig. 4E), and increase the number of platforms crossing times (Fig. 4F) in aged mice, indicating the positive effects of these EVs on spatial learning and memory abilities. USC-EVs-Y, USC-EVs-A, and USC-EVs-O could also notably increase the latency of mice to fall from the iron rod, the speed to cross the balance beam, and the latency to fall from the rotarod, as revealed by the grip strength test (Fig. 4G), the balance beam test (Fig. 4H), and the rotarod test (Fig. 4I), respectively, indicating that USC-EVs from different donors can enhance muscle strength and motor function of aged mice. No significant differences were detected in the above parameters among three types of USC-EVs groups (Fig. 4D−I). μCT analysis and three-point bending test of the femurs showed that all these USC-EVs could markedly improve most of the bone microstructural parameters (including Tb. BV/TV, Tb. Th, Tb. N, and Ct. Th) and increase the femur ultimate load in aged mice (Fig. 4J−L). USC-EVs-A exhibited slightly higher anti-osteoporotic effects compared with USC-EVs-Y and USC-EVs-O, because just USC-EVs-A not only had a profound negative effect on Tb. Sp, but also induced a significant positive effect on PS. Pm (Fig. 4J and K). However, there were no statistical differences in the positive effects of these EVs on bone mass and strength (Fig. 4J−L).

Senescent cell staining showed that USC-EVs-Y, USC-EVs-A, and USC-EVs-O could all remarkably reduce cellular senescence in the hippocampus, femur, muscle, heart, and skin tissues, as revealed by the much lower mean intensity for SA-β-gal-positive cells in the hippocampus (Fig. 5A and B), fewer p16^{INK4a}-positive cells in the SGZ site of the hippocampus (Fig. 5C and D), and lower mean intensity for P21^{Cip1}-positive cells in the femur, muscle, heart, and skin tissues (Fig. 5E and F). TUNEL staining showed that treatment with these EVs resulted in a significant reduction of apoptotic cell number in the aged bone tissues (Fig. 5G and H). H&E staining, COL17A1 immunostaining, and Masson's trichrome staining, respectively, showed that these EVs were also able to notably increase muscle fiber size (Supporting Information Fig. S5A and Fig. 5I), stimulate skin COL17A1 expression (Fig. S5B and Fig. 5J), augment skin collagen deposition, and enhance dermal thickness (Fig. S5C and Fig. 5K) in natural aging mice. In addition, treatment with these different donor-derived USC-EVs induced remarkable decreases in the circulating levels of SASP factors in aged mice (Fig. 5L). No obvious differences were detected in the abilities of USC-EVs-Y, USC-EVs-A, and USC-EVs-O to attenuate aging-related phenotypes in different tissues (Fig. S5A−S5C and Fig. 5A−K) and reduce the levels of the systemic SASP factors (Fig. 5L).

3.4. PLAU and TIMP1 are enriched in USC-EVs and contribute to the anti-aging effects of USC-EVs in senescent cells

We previously performed proteomic analysis to identify proteins expressed in USC-EVs and USCs from the above-mentioned 28-year-old woman[16]. In this and subsequent studies, we determined the function of several proteins highly enriched in USC-EVs[14−16]. We further analyzed the proteomic data and screened the proteins that might mediate the anti-aging effects of USC-EVs. In the proteins that have been proven to have anti-aging effects, the top five most abundant proteins in USC-EVs compared with USCs were PLAU (E/C = 38.42 ± 2.82-fold), TIMP1 (E/C = 35.34 ± 7.66-fold), IGFBP5 (E/C = 23.17 ± 2.25-fold), SMP30 (E/C = 14.72 ± 1.21-fold), and CTGF (E/C = 9.13 ± 2.49-fold) (Fig. 6A). We selected the top two most abundant proteins (PLAU and TIMP1) for further exploration. Western blotting revealed that both of these two proteins were detected in these nine donors-derived USC-EVs, but no age-related reduction of these proteins was observed (Supporting Information Fig. S6).

To examine whether PLAU and TIMP1 were responsible for the anti-aging effects of USC-EVs, these two proteins in USC-EVs were down-regulated by inhibiting their genes in USCs using the respective shRNAs. The inhibitory effects of three shRNAs targeting PLAU or TIMP1 in USCs were compared by quantitative real-time PCR (qRT-PCR) analysis. As shown in Fig. 6B, shPLAU #3 and shTIMP1 #1 exhibited the highest efficiency of inhibiting PLAU and TIMP1, respectively. Western blotting revealed that the inhibition of PLAU and TIMP1 in USCs successfully suppressed the levels of these proteins in their derived EVs (USC^{shPLAU}-EVs and USC^{shTIMP1}-EVs), as compared to USC^{shCon}-EVs (Fig. 6C). SA-β-gal staining revealed that the inhibition of either one of these two proteins especially PLAU resulted in significantly reduced abilities of USC-EVs to reverse hydrogen peroxide-induced senescence of HL-1, HSF, C2C12, and BMSCs (Fig. 6D and E). The inhibitory effect on serum deprivation-induced senescence and stimulatory effect on neurite growth of CAD cells were also markedly repressed with the down-regulation of either of these two proteins especially PLAU in USC-EVs (Fig. 6F and G). Flow cytometry with Annexin V-FITC/PI staining revealed that knockdown of PLAU or TIMP1 markedly impaired the anti-apoptotic capacity of USC-EVs (Supporting Information Fig. S7 and Fig. 6H). Suppression of either PLAU or TIMP1 did not entirely abolish the anti-senescent, neurite growth-promoting, and anti-apoptotic effects of USC-EVs (Fig. 6D−H and Fig. S7). These results indicate that PLAU and TIMP1 partially mediate the protective effects of USC-EVs in senescent cells.

3.5. Inhibition of MMPs, P16^{INK4a}, and P21^{Cip1} by PLAU and TIMP1 contributes to the anti-senescent effects of USC-EVs

Senescent cells can secrete MMPs as part of their SASP factors and subsequently re-enforce senescence though an autocrine or paracrine manner[38]. The MMPs such as MMP1 and MMP12 have been reported to be capable of inducing cellular senescence[38,39]. Since TIMP1 is a potent inhibitor of MMPs, we then assessed the expression changes of MMP1 and MMP12 in different cell types treated with vehicle, TIMP1 recombinant protein, USC^{shCon}-EVs, or USC^{shTIMP1}-EVs under senescence induction by hydrogen peroxide. The effects of PLAU protein and USC^{shPLAU}-EVs on the expression of these two MMPS were also evaluated. Western blotting revealed that incubation with TIMP1 protein or USC^{shCon}-EVs significantly reduced the protein levels of MMP1 and MMP12 in senescent HL-1, C2C12, and BMSCs (Fig. 7A). However, the reductions of these two MMPs were not significant in the above-described senescent cells treated with TIMP1-lacking USC-EVs (USC^{shTIMP1}-EVs), but not USC^{shPLAU}-EVs (Fig. 7A). We also assessed the protein levels of the senescence marker

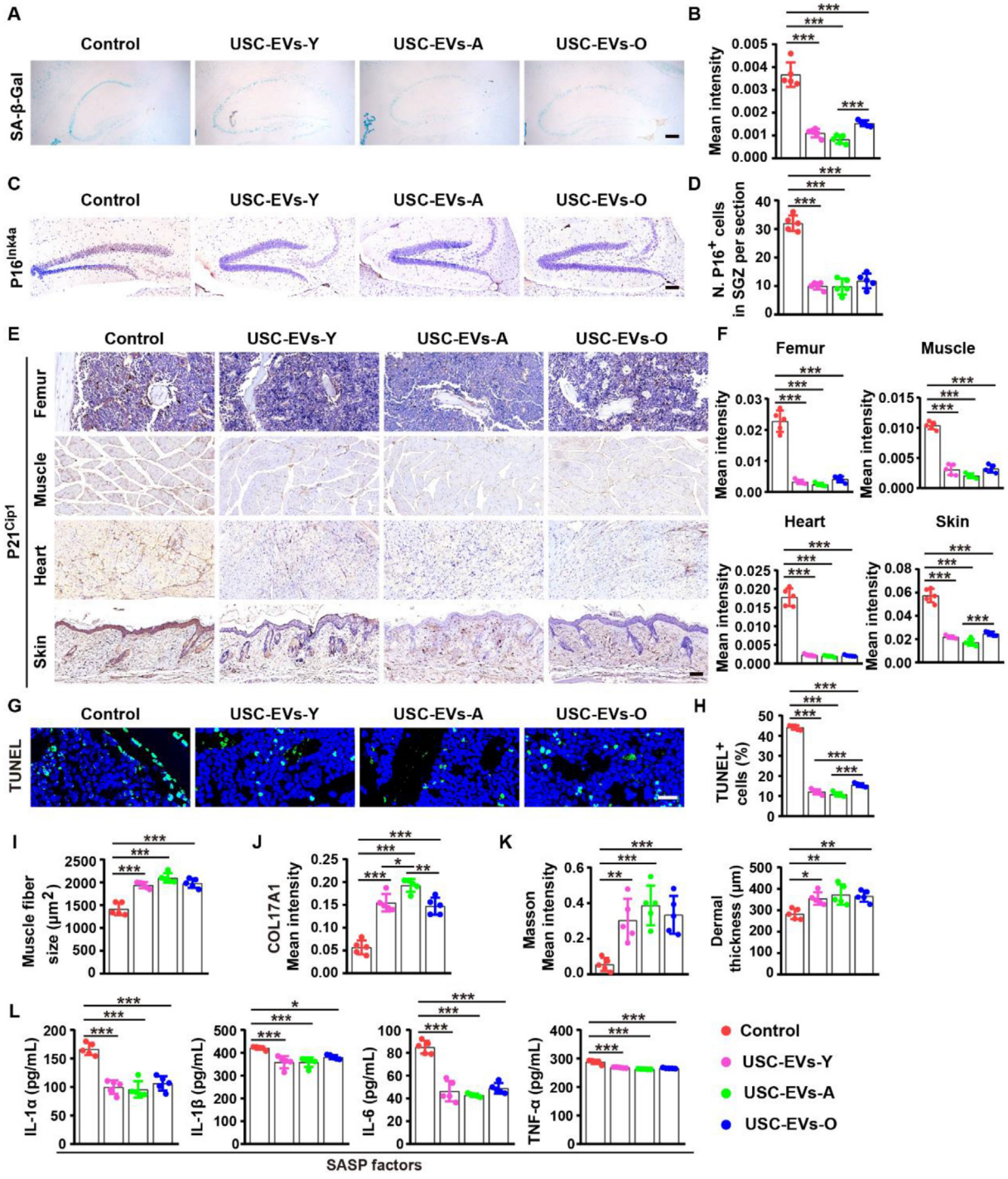

Figure 5 Multiple donor-derived USC-EVs attenuate aging-related phenotypes in different organs of natural aging mice. (A, B) SA-β-gal staining images of the hippocampus (A) and quantification of the mean intensity for the positive signals (B) in natural aging mice treated with vehicle or USC-EVs from different donors. Scale bar: 500 μm. $n = 5$ per group. (C, D) Immunostaining images of $P16^{INK4a}$ in SGZ region of the hippocampus (C) and quantification of the mean staining intensity for $P16^{INK4a}$ in natural aging mice with different treatments. Scale bar: 100 μm. $n = 5$ per group. (E, F) Immunostaining images of $P21^{Cip1}$ in different tissues (E) and quantification of the mean staining intensity for $P21^{Cip1}$ (F) in natural aging mice with different treatments. Scale bar: 50 μm (for femurs) or 100 μm (for other tissues). $n = 5$ per group. (G, H) TUNEL staining images (G) and quantification of the number of apoptotic cells (H) in bone tissues of the natural aging mice with different treatments. Scale bar: 20 μm. $n = 5$ per group. (I) Quantification of the size of the H&E-stained muscle fibers in natural aging mice with different treatments. $n = 5$ per group. (J) Quantification of the mean staining intensity for COL17A1 in skin tissues of natural aging mice receiving different treatments. $n = 5$ per group. (K) Quantification of the mean staining intensity for the Masson's trichrome-stained collagen fibers and dermal thickness in natural aging mice with different treatments. $n = 5$ per group. (L) Evaluation of the serum concentrations of SASP factors in natural aging mice with different treatments by ELISA. $n = 5$ per group. Data are shown as mean ± SD. $^*P < 0.05$, $^{**}P < 0.01$, $^{***}P < 0.001$.

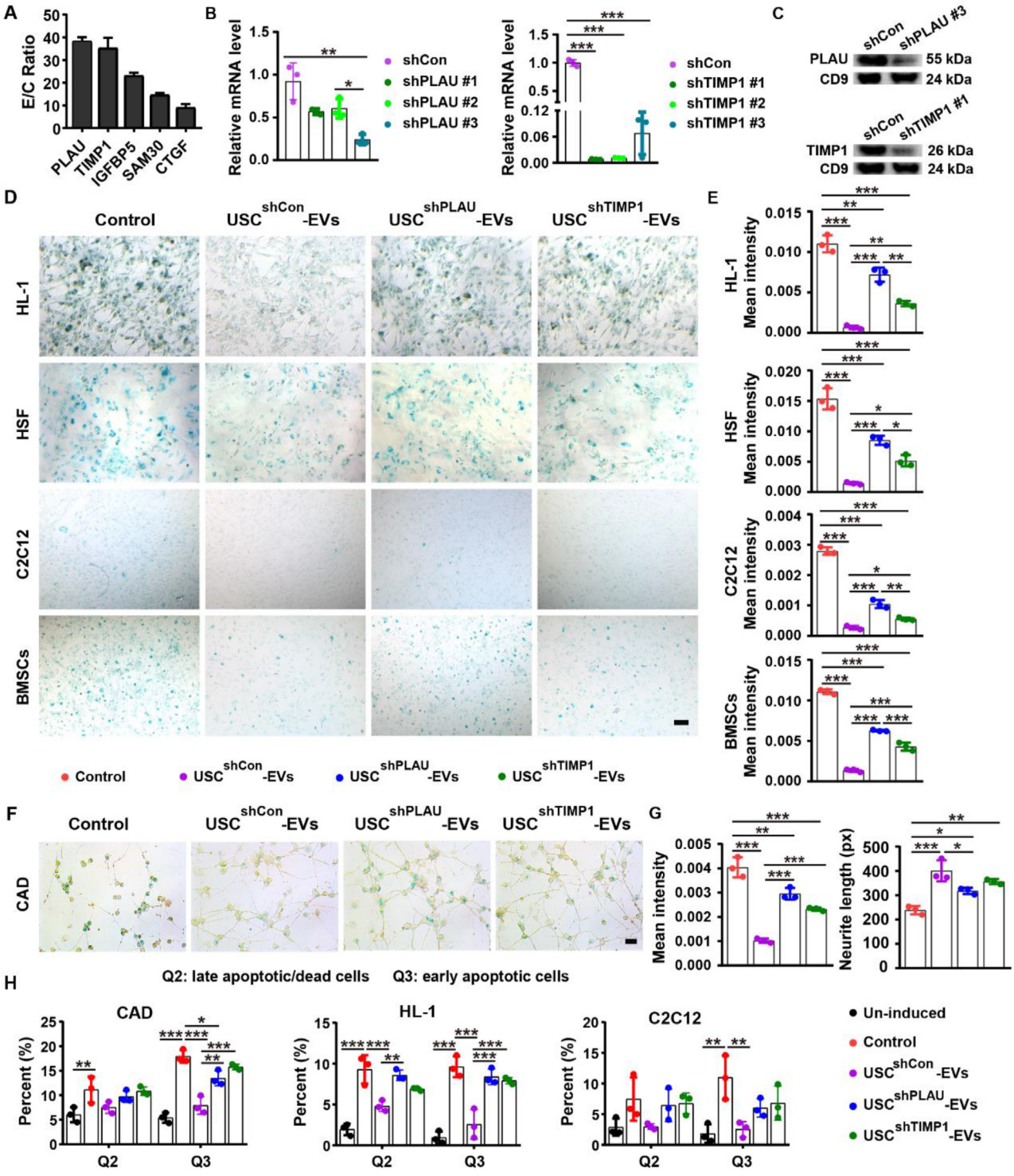

Figure 6 PLAU and TIMP1 are enriched in USC-EVs and contribute to the anti-aging effects of USC-EVs in senescent cells. (A) Expression ratios of the top five most abundant anti-aging proteins in USC-EVs (E) compared with USCs (C) assessed by proteomic analysis. $n = 3$ per group. (B) Inhibitory efficiency of shRNAs targeting PLAU or TIMP1 in USCs by qRT-PCR. $n = 3$ per group. (C) Down-regulation efficiency of PLAU and TIMP1 in USC-EVs detected by Western blotting. (D) SA-β-gal staining images of different cell types in hydrogen peroxide containing medium added with vehicle, USC^{shCon}-EVs, USC^{shPLAU}-EVs, or USC^{shTIMP1}-EVs. Scale bar: 50 μm. (E) Quantification of the mean intensity for the SA-β-gal-stained cells. $n = 3$ per group. (F) SA-β-gal staining images of CAD cells treated with vehicle, USC^{shCon}-EVs, USC^{shPLAU}-EVs, or USC^{shTIMP1}-EVs in serum-free condition. Scale bar: 50 μm. (G) Quantification of the mean intensity for the SA-β-gal-stained cells and the length of neurites. $n = 3$ per group. (H) Quantification of the percent of late apoptotic/dead cells (Q2) and early apoptotic cells (Q3) tested by flow cytometry with annexin V-FITC/PI staining. $n = 3$ per group. Data are shown as mean ± SD. $^*P < 0.05$, $^{**}P < 0.01$, $^{***}P < 0.001$.

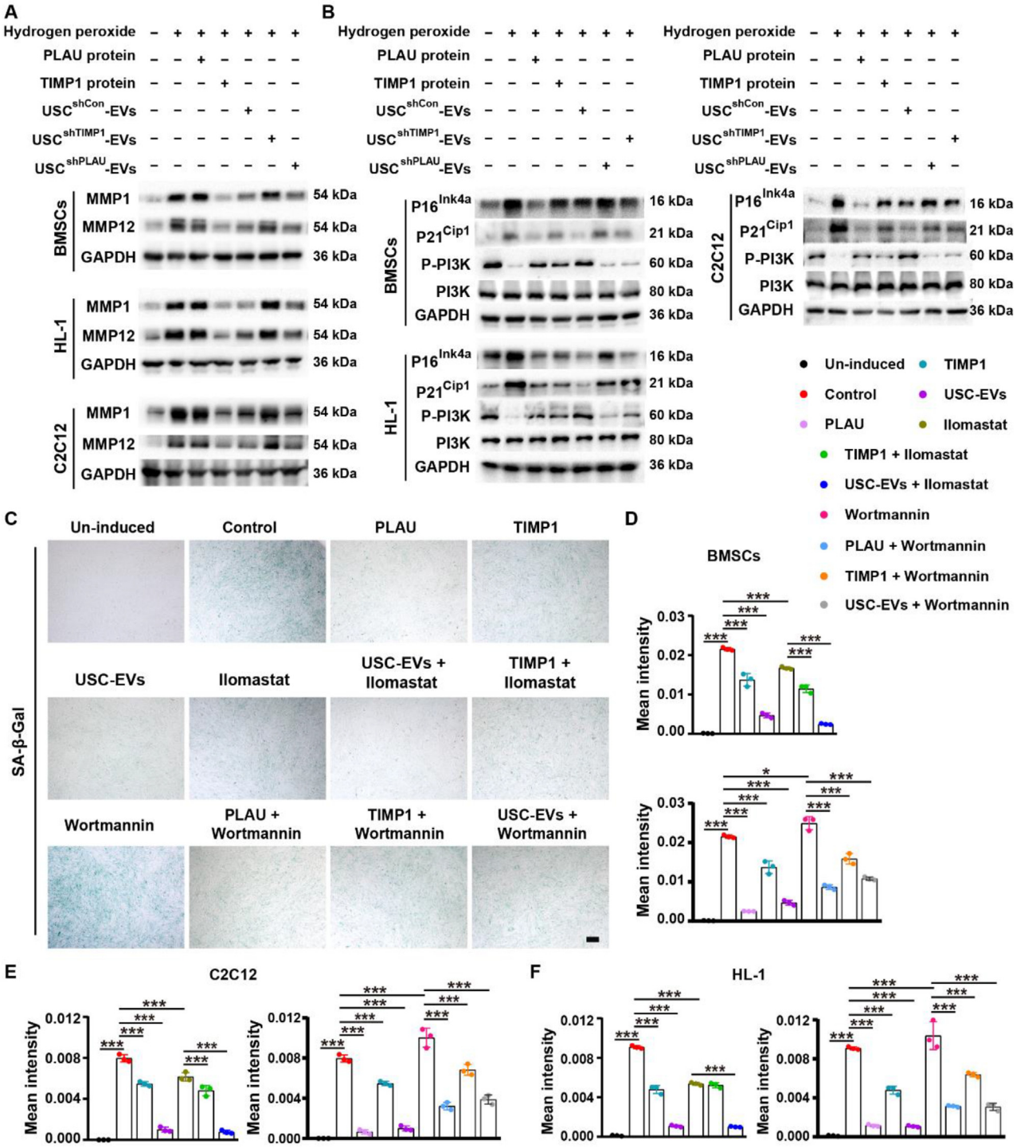

Figure 7 Inhibition of MMPs, $P16^{INK4a}$, and $P21^{Cip1}$ by PLAU and TIMP1 contributes to the anti-senescent effects of USC-EVs. (A, B) Western blot analysis of the protein expression of MMP1, MMP12, $P16^{INK4a}$, $P21^{Cip1}$, P-PI3K, and PI3K in HL-1, C2C12, and BMSCs receiving different treatments under senescence induction by hydrogen peroxide. (C) SA-β-gal staining images in BMSCs receiving different treatments under senescence induction by hydrogen peroxide. Scale bar: 50 μm. (D)−(F) Quantification of the mean intensity for the SA-β-gal-stained cells in BMSCs (D), C2C12 (E), and HL-1 (F) receiving different treatments under senescence induction by hydrogen peroxide. $n = 3$ per group. Data are shown as mean ± SD. $^*P < 0.05$, $^{***}P < 0.001$.

$P16^{INK4a}$ and $P21^{Cip1}$, which are involved in inducing senescence[40]. The result showed that these senescence markers were remarkably increased in BMSCs, HL-1, and C2C12 after exposure to hydrogen peroxide, whereas this alteration was profoundly suppressed by PLAU, TIMP1, and USC^{shCon}-EVs (Fig. 7B). USC^{shPLAU}-EVs and $USC^{shTIMP1}$-EVs exhibited markedly reduced abilities to down-regulate $P16^{INK4a}$ and $P21^{Cip1}$ proteins in the above-described cells compared with USC^{shCon}-EVs

(Fig. 7B), suggesting that the anti-senescent effects of PLAU, TIMP1, and these two proteins-abundant USC-EVs are exerted by targeting $P16^{INK4a}$- and $P21^{Cip1}$-dependent pathways. Phosphoinositide-3 kinase-protein kinase B (PI3K−Akt) signaling is involved in the regulation of cellular senescence[41] and can be activated by PLAU[42] and TIMP1[43]. Western blotting revealed that hydrogen peroxide treatment resulted in a marked reduction of PI3K phosphorylation in BMSCs, HL-1, and C2C12, whereas this change was notably reversed by co-incubation with PLAU, TIMP1, or USC^{shCon}-EVs (Fig. 7A and B). The capacity of USC^{shPLAU}-EVs and $USC^{shTIMP1}$-EVs to enhance PI3K phosphorylation was much lower than that of USC^{shCon}-EVs (Fig. 7A and B).

Ilomastat, a broad-spectrum inhibitor of MMPs, was used to interfere with the function of MMPs. SA-β-gal staining showed that treatment with either Ilomastat, TIMP1 protein, or USC-EVs markedly suppressed the hydrogen peroxide-induced senescence of the above three cell types (Fig. 7C−F). USC-EVs and TIMP1 protein could still suppress senescence in the Ilomastat-treated BMSCs, but their anti-senescent effects, especially those of TIMP1 protein, were notably impaired (Fig. 7C−F), suggesting that the inhibition of MMPs by TIMP1 is a critical mechanism by which USC-EVs exert anti-senescent effects. We further assessed whether the inhibition of PI3K−Akt signaling by a commercial inhibitor, wortmannin, could affect the anti-senescent effects of USC-EVs. SA-β-gal staining revealed that wortmannin increased the hydrogen peroxide-induced cellular senescence, and additional treatment with USC-EVs, PLAU, or TIMP1 further reduced cellular senescence in the wortmannin-treated cells (Fig. 7C−F). The extent of cellular senescence inhibition by PLAU, TIMP1, and USC-EVs was not notably affected by wortmannin (Fig. 7C−F), suggesting that PI3K−Akt signaling is not involved in the USC-EVs and their enriched proteins PLAU- and TIMP1-induced inhibitory effects against cellular senescence.

3.6. PLAU and TIMP1 mediate the anti-aging activity of USC-EVs in natural aging mice

To determine the roles of PLAU and TIMP1 in the anti-aging activity of USC-EVs *in vivo*, 16-month-old C57BL/6J mice were intravenously injected with USC^{shPLAU}-EVs, $USC^{shTIMP1}$-EVs, USC^{shCon}-EVs, or vehicle once a week for 12 weeks. MWM test showed that the administration of USC^{shPLAU}-EVs or $USC^{shTIMP1}$-EVs to the mice just induced a significant reduction of the latency to escape onto the platform on Day 1 and trend of increases in target quadrant occupancy or/and platform crossing times, whereas the mice treated with USC^{shCon}-EVs showed markedly reduced escape latency from Day 1 to Day 5 as well as notably higher time in target quadrant and number of crossing times through the platform compared to the control mice (Fig. 8A−C). Suppression of either one of these two proteins especially PLAU also significantly impaired, but did not entirely block, the abilities of USC-EVs to increase the latency to fall in the grip test (Fig. 8D), the crossing speed in the balance beam test (Fig. 8E), and the latency to fall in the rotarod test (Fig. 8F). μCT analysis and three-point bending test of the femurs showed that USC^{shPLAU}-EVs and $USC^{shTIMP1}$-EVs exhibited much lower capacities to reduce Tb. Sp and enhance Tb. BV/TV, Tb. N, Ct. Th, and ultimate load values compared with USC^{shCon}-EVs (Fig. 8G−I). However, USC^{shPLAU}-EVs and $USC^{shTIMP1}$-EVs still could induce significant changes of many of these parameters, as compared with the vehicle group (Fig. 8G−I). These results indicate that PLAU and TIMP1 partially mediate the positive effects of USC-EVs on spatial learning and memory abilities, motor function, bone mass, and bone strength in aged mice.

Senescent cell staining showed that treatment with USC^{shPLAU}-EVs or $USC^{shTIMP1}$-EVs caused significant reductions in the mean intensity for SA-β-gal-positive cells in the hippocampus (Fig. 9A and B), the number of $P16^{INK4a}$-positive cells in the SGZ site of the hippocampus (Fig. 9C and D), and the mean intensity for $P21^{Cip1}$-positive cells in the femur, muscle, heart, and skin tissues of natural aging mice (Fig. 9E and F), whereas their anti-senescent effects in these tissues were much lower compared with USC^{shCon}-EVs (Fig. 9A−F). TUNEL staining showed that the down-regulation of PLAU or TIMP1 in USC-EVs markedly suppressed the anti-apoptotic effect of USC-EVs in the aged bone tissues (Fig. 10A and B). Inhibition of PLAU or TIMP1 also notably impaired the abilities of USC-EVs to increase muscle fiber size (Fig. 10C and D), skin COL17A1 expression (Fig. 10E and F), skin collagen deposition, and dermal thickness (Fig. 10G and H) in aged mice. However, the suppression of positive effects of USC-EVs on muscle fiber size and skin COL17A1 expression was much obvious with the inhibition of PLAU (Fig. 10C−F). Additionally, down-regulation of either one of these two proteins especially PLAU profoundly repressed the negative effects on systemic SASP factor generation (Fig. 10I). These results further determine the critical contribution of PLAU and TIMP1 to the anti-aging properties of USC-EVs.

Collectively, in our study, we isolated USCs from human urine and then collected USC-EVs for assessing their anti-aging effects in aged mice after intravenous injection (Fig. 11). Our results showed that USC-EVs could reduce senescent cell burden and improve the structure and function of different organs (brain, bone, muscle, heart, and skin) in aged mice by transferring PLAU and TIMP1 proteins, thereby reverting the old organ towards a more “youthful” state (Fig. 11).

4. Discussion

Aging is defined as a gradual loss of biological integrity with time due to accumulation of molecular and cellular damage, which finally leads to decreased physiological function and increased vulnerability to death[4,44]. Developing strategies for delaying the aging process and the onset and progression of age-associated disorders would have tremendous health and financial benefits[44]. Various strategies show promise to slow aging and extend healthspan and lifespan, but only a few of them can be explored for clinical practice due to the long validation times[44]. In this study, we harvested stem cells from human urine and determined that their EVs (USC-EVs) could prevent cellular senescence, promote neurite growth, and mitigate age-associated functional decline and/or structural changes in various tissues. Surprisingly, there was no USC donor’s age-related significant reduction of the anti-aging properties of USC-EVs, and there were also no regular changes of the anti-aging effects of USC-EVs from donors with different genders or health status (healthy or with age- and menopause-related osteoporosis), consistent with our previous findings that the bone-protective capacity of USC-EVs is not markedly affected by the USC donor’s age, gender, and health conditions[14]. These results, along with the advantages of EV-based therapy, suggest the great potential of autologous USC-EVs as a promising agent for anti-aging and rejuvenation. Nevertheless, future studies are required much larger sample sizes to compare

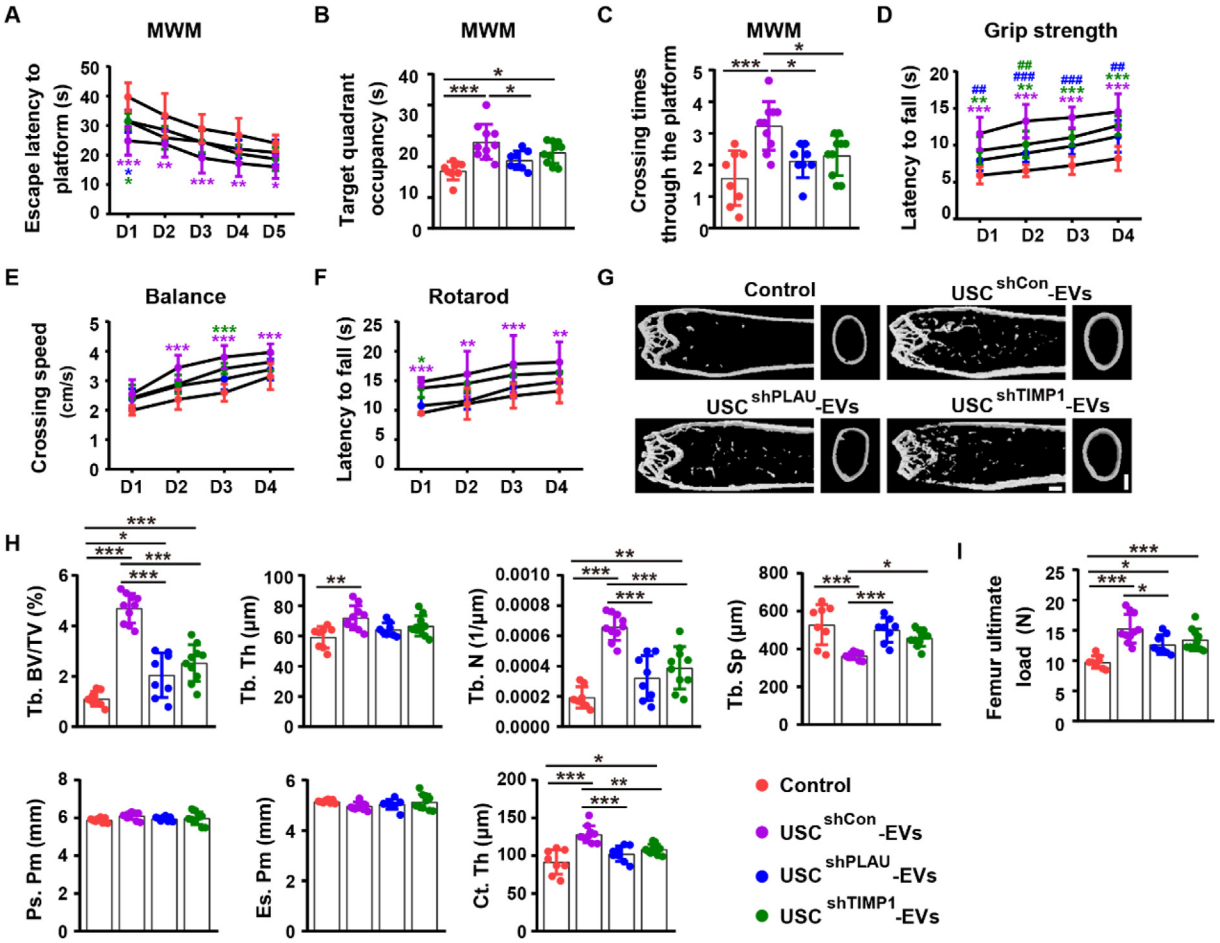

Figure 8 Downregulation of PLAU and TIMP1 weakens the benefits of USC-EVs on behavioral responses and bone quality in natural aging mice. (A)−(C) MWM test of the spatial learning and memory abilities of the natural aging mice treated with vehicle, USC^{shCon}-EVs, USC^{shPLAU}-EVs, or USC^{shTIMP1}-EVs. $n = 8-10$ per group. (D)−(F) Muscle strength and motor function assessments by grip strength test (D), balance beam test (E), and rotarod test (F) in natural aging mice treated with vehicle, USC^{shCon}-EVs, USC^{shPLAU}-EVs, or USC^{shTIMP1}-EVs. $n = 8-10$ per group. (G, H) μCT-reconstructed images of the femurs (G) and quantification of the trabecular and cortical bone microstructural parameters (H) in natural aging mice treated with vehicle, USC^{shCon}-EVs, USC^{shPLAU}-EVs, or USC^{shTIMP1}-EVs. Scale bar: 1 mm. $n = 8-10$ per group. (I) Three-point bending test of the femur strength in natural aging mice treated with vehicle, USC^{shCon}-EVs, USC^{shPLAU}-EVs, or USC^{shTIMP1}-EVs. $n = 8-10$ per group. Data are shown as mean ± SD. For panel (D): $^{*}P < 0.05$ *vs.* Control group and $^{\#}P < 0.05$ *vs.* USC^{shCon}-EVs group. $^{*/\#}P < 0.05$, $^{**/\#\#}P < 0.01$, $^{***/\#\#\#}P < 0.001$. For other panels: $^{*}P < 0.05$, $^{**}P < 0.01$, $^{***}P < 0.001$.

the *in vivo* anti-aging effects of USC-EVs from donors of different age, gender, and health conditions, which will be better for determining the factors affecting the function of USC-EVs. Furthermore, USC-EVs used in our study were isolated from the cultured USCs that had been away from their *in vivo* microenvironment. It remains to be further investigated whether the anti-aging capacity of the endogenous USC-EVs from USCs resident in the body is reduced with age.

Cellular senescence contributes greatly to aging and aging-related diseases. Emerging evidence indicates that neuronal cells, BMSCs, cardiomyocytes, myoblast cells, and fibroblasts, can become senescent with age and play critical roles in the aging of the related organs, leading to cognitive function impairment[45,46], osteoporosis[47], cardiac failure[48], muscle dysfunction[49], and reduction of collagen and dermal thickness[50], respectively. In our study, we found that treatment with USC-EVs markedly inhibited serum deprivation-induced senescence of mouse neuronal cell line CAD, and hydrogen peroxide-induced senescence of mouse primary BMSCs, mouse cardiomyocyte cell line HL-1, mouse myoblast cell line C2C12, and human skin fibroblasts. Consistently, the results *in vivo* indicated that the administration of USC-EVs into the aged mice notably suppressed cellular senescence in the brain, bone, heart, muscle, and skin. The above findings suggest that the suppression of cellular senescence is an important mechanism by which USC-EVs exert anti-aging effects in the mice, such as improving cognitive function, enhancing muscle strength, increasing bone density, etc. Other pathways may also be involved in the anti-aging properties of USC-EVs. Increased cellular apoptosis occurs with the aging of various organs[31,32]. We found that treatment with USC-EVs profoundly decreased cellular apoptosis both in the cultured cells and the brain of the aged mice, suggesting that the suppression of cellular apoptosis may also contribute to the benefits of USC-EVs in the aged organs. Impaired angiogenesis and endothelial dysfunction contribute to the increased prevalence of cardiovascular aging muscle weakness, and bone loss in the elderly[51−53]. Our previous study has

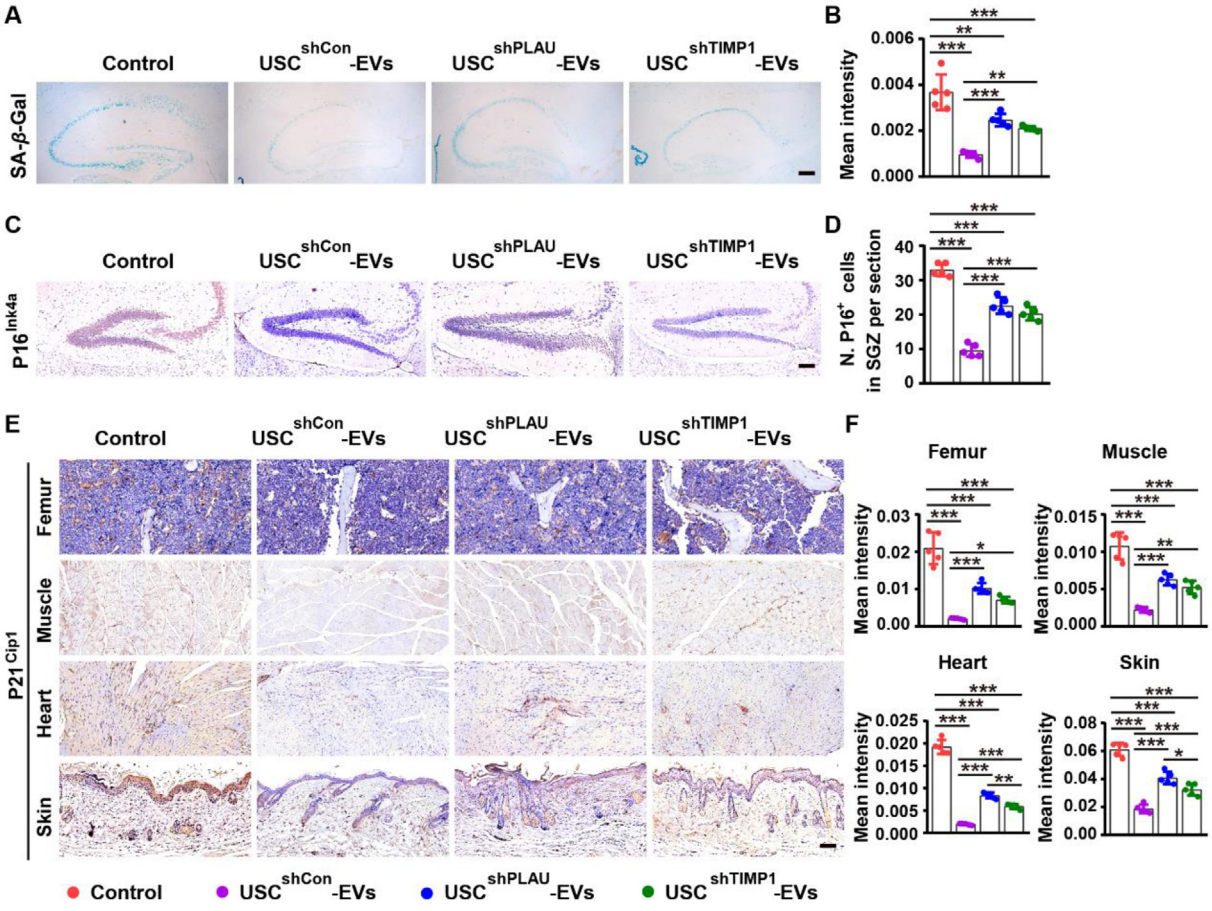

Figure 9 PLAU and TIMP1 mediate the inhibitory effects USC-EVs on cellular senescence in different organs of natural aging mice. (A, B) SA-β-gal staining images of the hippocampus (A) and quantification of the mean staining intensity (B) in natural aging mice treated with vehicle, USC^{shCon}-EVs, USC^{shPLAU}-EVs, or USC^{shTIMP1}-EVs. Scale bar: 500 μm. $n = 5$ per group. (C, D) Immunostaining images of P16^{INK4a} in SGZ region of the hippocampus (C) and quantification of the mean staining intensity (D) in natural aging mice from (A). Scale bar: 100 μm. $n = 5$ per group. (E, F) Immunostaining images of P21^{Cip1} in femur, muscle, heart, and skin tissues (E) and quantification of the mean staining intensity (F) in natural aging mice with different treatments. Scale bar: 50 μm (for femurs) or 100 μm (for other tissues). $n = 5$ per group. Data are shown as mean ± SD. $^{*}P < 0.05$, $^{**}P < 0.01$, $^{***}P < 0.001$.

shown that USC-EVs can enhance angiogenesis in the wounds by transferring pro-angiogenic proteins to endothelial cells[16]. There is a possibility that the promotion of angiogenesis may also be a contributing factor to the anti-aging effects of USC-EVs, which warrants future exploration.

PLAU is a secreted serine protease that is also called urokinase-type plasminogen activator and shares conserved functional domains among different mammalian species[54]. This protein cleaves plasminogen to plasmin, which is also a serine protease that can hydrolyze fibrin clots and various proteins in the extracellular matrix (ECM)[26]. PLAU plays important roles in vascular remodeling[55], nerve repair/regeneration[56], inflammation[57], and aging[26,42,58,59]. Overexpression of PLAU or down-regulation of plasminogen activator inhibitor-1 can induce senescence bypass in fibroblasts[42]. Transgenic mice over-expressing PLAU in the brain exhibit markedly reduced food consumption and body weight, longer lifespan, and much slower age-related declines in wound healing and cardia function compared with the wild-type mice[26,58,59]. EVs are key mediators of intercellular communication by interacting with target cells and then unloading cargos into their recipient cells to modulate cell activity. In this study, we found that PLAU protein was accumulated in USC-EVs and partly mediated the anti-aging effects of USC-EVs both *in vitro* and *in vivo*. Even though PLAU negatively modulates food intake and body weight[26,58,59], the USC-EVs-treated mice did not show symptoms of anorexia and weight loss (data not shown). That may be because some other molecules in USC-EVs exert positive effects on food intake and weight growth opposite to those exerted by PLAU.

TIMP1 is a secretory glycoprotein that inhibits MMPs, a group of conserved peptidases that degrade ECM proteins[60]. TIMP1 also inhibits cell apoptosis[61], promotes cell proliferation[62], and benefits bone health[63]. Previous studies have shown that the expression of TIMP1 is reduced with skin natural aging or photoaging and this alteration contributes to dermal ECM degradation and decreased cell proliferation and survival in aged skin[25,64]. Overexpression of TIMP1 leads to a profound inhibition of ultraviolet B radiation-induced cutaneous photoaging[64]. In the present study, we determined that this protein was highly enriched in USC-EVs and acted as an important contributor to the USC-EVs-induced inhibitory effects on cellular senescence and age-related functional and structural changes. Previously, we have shown that TIMP1 is

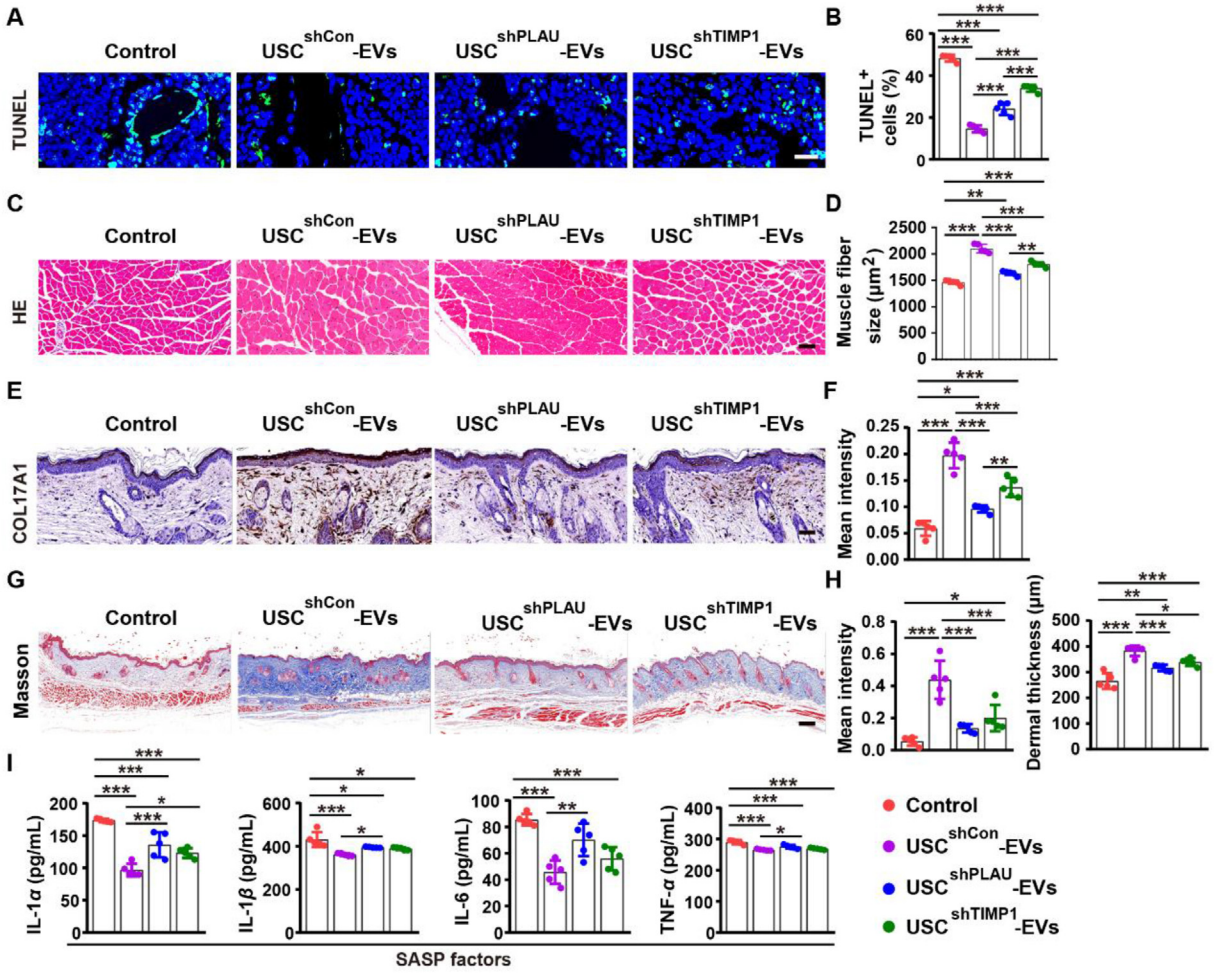

Figure 10 PLAU and TIMP1 contribute to the USC-EVs-induced suppression of various aging-related phenotypes in different organs of natural aging mice. (A, B) TUNEL staining images (A) and quantification of apoptotic cell number (B) in bone tissues of the natural aging mice with different treatments. Scale bar: 20 μm. $n = 5$ per group. (C, D) H&E staining images of muscle tissues (C) and quantification of muscle fiber size (D) in natural aging mice with different treatments. Scale bar: 100 μm. $n = 5$ per group. (E, F) Immunohistochemical staining for COL17A1 in skin tissues (E) and quantification of the mean staining intensity (F) in natural aging mice with different treatments. Scale bar: 50 μm. $n = 5$ per group. (G, H) Masson's trichrome staining of skin tissues (G) and quantification of the mean staining intensity as well as dermal thickness (H) in natural aging mice with different treatments. Scale bar: 200 μm. $n = 5$ per group. (I) Evaluation of the serum concentrations of SASP factors in natural aging mice with different treatments by ELISA. $n = 5$ per group. Data are shown as mean ± SD. $^{*}P < 0.05$, $^{**}P < 0.01$, $^{***}P < 0.001$.

required for the protective effects of USC-EVs against glucocorticoid-induced cell apoptosis and osteonecrosis[15]. Thus, in addition to its direct negative role in cellular senescence, the influences on other processes such as the inhibition of cell apoptosis and the augmentation of bone cell function may be also involved in the TIMP1-mediated anti-aging effects of USC-EVs.

The benefits of EVs are exerted by transferring multi-functional factors, but not just by a single or two factors[14,15,17,21]. Our results revealed that the inhibition of PLAU or TIMP1 did not completely abolish the USC-EVs-induced anti-aging effects, which might be due to the fact that USC-EVs also contained other molecules possessing anti-aging capacities, such as insulin-like growth factor binding protein 5[27], senescence marker protein-30[28], and connective tissue growth factor[29]. It remains to be investigated whether these proteins in USC-EVs can rejuvenate senescent cells and delay the aging process in aged body. Besides the anti-senescent proteins, other molecules may also make contributions to the USC-EVs-induced beneficial effects in aged mice. We have previously determined that USC-EVs alleviate ovariectomy-induced osteoporosis associated with the transfer of pro-osteogenic and anti-osteoclastic proteins including collagen triple-helix repeat containing 1 and osteoprotegerin[14]. These molecules may also contribute to the USC-EVs-induced improvements of bone mass and bone strength in aged mice, which still needs future exploration. Another limitation in our study is that we did not further explore why the above-described functional proteins such as PLAU and TIMP1 were highly enriched in USC-EVs. Future studies are also worthwhile to investigate the detailed molecular mechanism that controls the specific enrichment of the anti-aging proteins in USC-EVs.

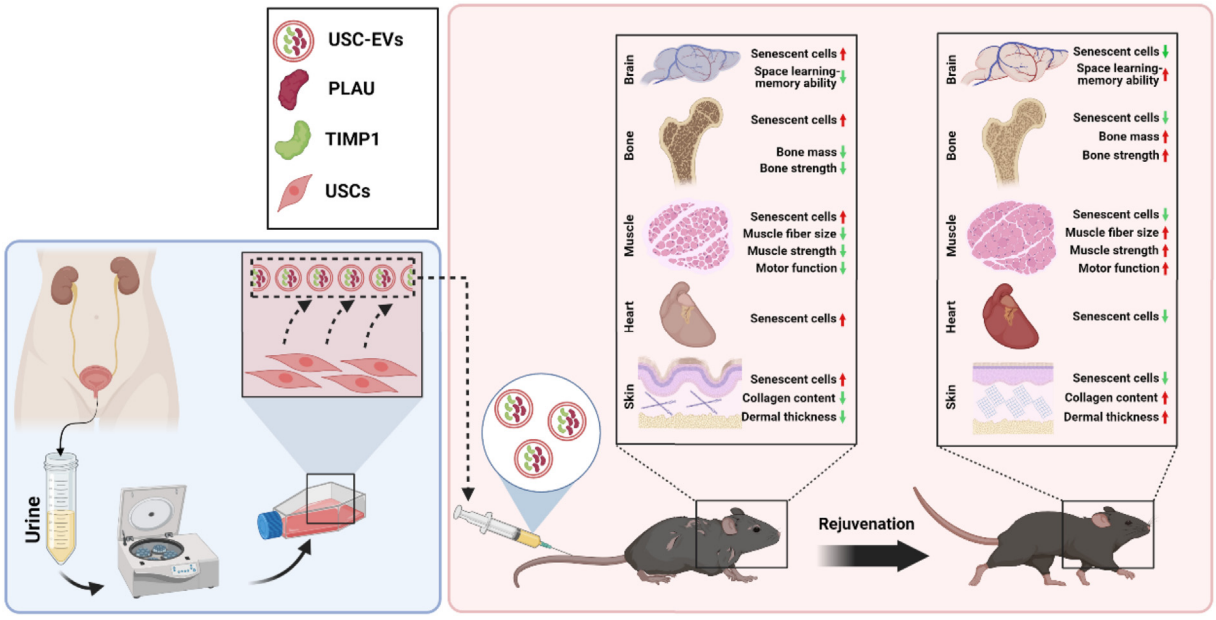

Figure 11 Schematic diagram showing human USC-EVs rejuvenate multiple old organs in aged mice through the transfer of PLAU and TIMP1 proteins. USCs were isolated from human urine and USC-EVs were collected from the culture medium of USCs. The intravenous administration of USC-EVs to aged mice reduced senescent cell burden and improved the structure and function of various organs by transferring PLAU and TIMP1 proteins, thereby rejuvenating the old organ towards a more "youthful" state.

5. Conclusions

Our study demonstrates that USC-EVs can efficiently delay multiple-organ aging and their anti-aging effects are not notably affected by the USC donors' ages, genders, or health status. The underlying mechanism is primarily the transfer of PLAU and TIMP1 protein, which down-regulated in USC-EVs significantly blocks their anti-aging effects. These findings suggest the promising potential of USC-EVs as an anti-aging agent by transferring PLAU and TIMP1.

Acknowledgments

This work was supported by the National Natural Science Foundation of China (Grant Nos. 82125023, 82072504, 81871822, 82172501, 81801395, and 82200039), the Science and Technology Innovation Program of Hunan Province (Grant Nos. 2020RC4008 and 2022RC1211, China), the China National Postdoctoral Program for Innovative Talents (Grant No. BX2021383, China), the Central South University Innovation-Driven Research Programme (Grant Nos. 2023CXQD001 and 2019CX014, China), the Hunan Province Natural Science Foundation of China (Grant Nos. 2023JJ10094 and 2020JJ5883), the Youth Science Foundation of Xiangya Hospital (Grant No. 2022Q07, China), and the Hunan Provincial Innovation Foundation for Postgraduate (Grant Nos. 2021ZZTS0342 and 2022ZZTS0239, China).

Author contributions

Chunyuan Chen, Hui Xie, and Siyuan Tang designed this study. Chunyuan Chen and Hui Xie wrote the manuscript. Shanshan Rao, Zehui He, Zun Wang, Hao Yin, Xiongke Hu, Yijuan Tan, Tengfei Wan, Hao Zhu, Yi Luo, Xin Wang, Hongming Li, Zhenxing Wang, Xinyue Hu, Chungu Hong, Yiyi Wang, Mingjie Luo, Wei Du, and Yuxuan Qian performed the experiments or/and analyzed the data. Shanshan Rao and Chunyuan Chen prepared the figures.

Conflicts of interest

The authors declare no conflicts of interest.

Appendix A. Supporting information

Supporting data to this article can be found online at https://doi.org/10.1016/j.apsb.2023.12.009.

References

1. Chaudhary M, Khan A, Gupta M. Skin ageing: pathophysiology and current market treatment approaches. *Curr Aging Sci* 2020;**13**:22–30.
2. Da Mesquita S, Herz J, Wall M, Dykstra T, de Lima KA, Norris GT, et al. Aging-associated deficit in CCR7 is linked to worsened glymphatic function, cognition, neuroinflammation, and β-amyloid pathology. *Sci Adv* 2021;**7**:eabe4601.
3. Hunt LC, Schadeberg B, Stover J, Haugen B, Pagala V, Wang YD, et al. Antagonistic control of myofiber size and muscle protein quality control by the ubiquitin ligase UBR4 during aging. *Nat Commun* 2021;**12**:1418.
4. López-Otín C, Blasco MA, Partridge L, Serrano M, Kroemer G. The hallmarks of aging. *Cell* 2013;**153**:1194–217.
5. Birch J, Gil J. Senescence and the SASP: many therapeutic avenues. *Genes Dev* 2020;**34**:1565–76.
6. Childs BG, Gluscevic M, Baker DJ, Laberge RM, Marquess D, Dananberg J, et al. Senescent cells: an emerging target for diseases of ageing. *Nat Rev Drug Discov* 2017;**16**:718–35.
7. Ren R, Ocampo A, Liu GH, Izpisua Belmonte JC. Regulation of stem cell aging by metabolism and epigenetics. *Cell Metab* 2017;**26**:460–74.
8. Li G, Zhu Q, Wang B, Luo R, Xiao X, Zhang Y, et al. Rejuvenation of senescent bone marrow mesenchymal stromal cells by pulsed triboelectric stimulation. *Adv Sci* 2021;**8**:e2100964.

9. Li J, Li SH, Dong J, Alibhai FJ, Zhang C, Shao ZB, et al. Long-term repopulation of aged bone marrow stem cells using young Sca-1 cells promotes aged heart rejuvenation. *Aging Cell* 2019;**18**:e13026.
10. Lavasani M, Robinson AR, Lu A, Song M, Feduska JM, Ahani B, et al. Muscle-derived stem/progenitor cell dysfunction limits healthspan and lifespan in a murine progeria model. *Nat Commun* 2012;**3**:608.
11. Chen CY, Rao SS, Yue T, Tan YJ, Yin H, Chen LJ, et al. Glucocorticoid-induced loss of beneficial gut bacterial extracellular vesicles is associated with the pathogenesis of osteonecrosis. *Sci Adv* 2022;**8**:eabg8335.
12. Liu JH, Chen CY, Liu ZZ, Luo ZW, Rao SS, Jin L, et al. Extracellular vesicles from child gut microbiota enter into bone to preserve bone mass and strength. *Adv Sci* 2021;**8**:2004831.
13. Kim DK, Bandara G, Cho YE, Komarow HD, Donahue DR, Karim B, et al. Mastocytosis-derived extracellular vesicles deliver miR-23a and miR-30a into pre-osteoblasts and prevent osteoblastogenesis and bone formation. *Nat Commun* 2021;**12**:2527.
14. Chen CY, Rao SS, Tan YJ, Luo MJ, Hu XK, Yin H, et al. Extracellular vesicles from human urine-derived stem cells prevent osteoporosis by transferring CTHRC1 and OPG. *Bone Res* 2019;**7**:18.
15. Chen CY, Du W, Rao SS, Tan YJ, Hu XK, Luo MJ, et al. Extracellular vesicles from human urine-derived stem cells inhibit glucocorticoid-induced osteonecrosis of the femoral head by transporting and releasing pro-angiogenic DMBT1 and anti-apoptotic TIMP1. *Acta Biomater* 2020;**111**:208−20.
16. Chen CY, Rao SS, Ren L, Hu XK, Tan YJ, Hu Y, et al. Exosomal DMBT1 from human urine-derived stem cells facilitates diabetic wound repair by promoting angiogenesis. *Theranostics* 2018;**8**:1607−23.
17. Hu G, Xia Y, Chen B, Zhang J, Gong L, Chen Y, et al. ESC-sEVs rejuvenate aging hippocampal NSCs by transferring SMADs to regulate the MYT1−Egln3−Sirt1 axis. *Mol Ther* 2021;**29**:103−20.
18. Gong L, Chen B, Zhang J, Sun Y, Yuan J, Niu X, et al. Human ESC-sEVs alleviate age-related bone loss by rejuvenating senescent bone marrow-derived mesenchymal stem cells. *J Extracell Vesicles* 2020;**9**:1800971.
19. Oh M, Lee J, Kim YJ, Rhee WJ, Park JH. Exosomes derived from human induced pluripotent stem cells ameliorate the aging of skin fibroblasts. *Int J Mol Sci* 2018;**19**:1715.
20. Liang JX, Liao X, Li SH, Jiang X, Li ZH, Wu YD, et al. Antiaging properties of exosomes from adipose-derived mesenchymal stem cells in photoaged rat skin. *BioMed Res Int* 2020;**2020**:6406395.
21. Sanz-Ros J, Romero-García N, Mas-Bargues C, Monleón D, Gordevicius J, Brooke RT, et al. Small extracellular vesicles from young adipose-derived stem cells prevent frailty, improve health span, and decrease epigenetic age in old mice. *Sci Adv* 2022;**8**:eabq2226.
22. Zhang Y, Kim MS, Jia B, Yan J, Zuniga-Hertz JP, Han C, et al. Hypothalamic stem cells control ageing speed partly through exosomal miRNAs. *Nature* 2017;**548**:52−7.
23. Kim YJ, Yoo SM, Park HH, Lim HJ, Kim YL, Lee S, et al. Exosomes derived from human umbilical cord blood mesenchymal stem cells stimulates rejuvenation of human skin. *Biochem Biophys Res Commun* 2017;**493**:1102−8.
24. Lei Q, Gao F, Liu T, Ren W, Chen L, Cao Y, et al. Extracellular vesicles deposit PCNA to rejuvenate aged bone marrow-derived mesenchymal stem cells and slow age-related degeneration. *Sci Transl Med* 2021;**13**:eaaz8697.
25. Hornebeck W. Down-regulation of tissue inhibitor of matrix metalloprotease-1 (TIMP-1) in aged human skin contributes to matrix degradation and impaired cell growth and survival. *Pathol Biol* 2003;**51**:569−73.
26. Miskin R, Masos T. Transgenic mice overexpressing urokinase-type plasminogen activator in the brain exhibit reduced food consumption, body weight and size, and increased longevity. *J Gerontol A Biol Sci Med Sci* 1997;**52**:B118−24.
27. Nojima I, Hosoda R, Toda Y, Saito Y, Ueda N, Horimoto K, et al. Downregulation of IGFBP5 contributes to replicative senescence *via* ERK2 activation in mouse embryonic fibroblasts. *Aging* 2022;**14**:2966−88.
28. Silva AMS, Socorro S, Hurtado de Llera A, Vaz CV, Correia S, Maia CJ. Overexpression of regucalcin mitigates the ageing-related changes in oxidative stress and sperm quality. *Theriogenology* 2020;**157**:472−82.
29. Itoh S, Hattori T, Tomita N, Aoyama E, Yutani Y, Yamashiro T, et al. CCN family member 2/connective tissue growth factor (CCN2/CTGF) has anti-aging effects that protect articular cartilage from age-related degenerative changes. *PLoS One* 2013;**8**:e71156.
30. Qi Y, Wang JK, McMillian M, Chikaraishi DM. Characterization of a CNS cell line, CAD, in which morphological differentiation is initiated by serum deprivation. *J Neurosci* 1997;**17**:1217−25.
31. Pollack M, Phaneuf S, Dirks A, Leeuwenburgh C. The role of apoptosis in the normal aging brain, skeletal muscle, and heart. *Ann N Y Acad Sci* 2002;**959**:93−107.
32. Tower J. Programmed cell death in aging. *Ageing Res Rev* 2015;**23**:90−100.
33. Zhang S, Chu WC, Lai RC, Lim SK, Hui JH, Toh WS. Exosomes derived from human embryonic mesenchymal stem cells promote osteochondral regeneration. *Osteoarthritis Cartilage* 2016;**24**:2135−40.
34. Hu Y, Rao SS, Wang ZX, Cao J, Tan YJ, Luo J, et al. Exosomes from human umbilical cord blood accelerate cutaneous wound healing through miR-21-3p-mediated promotion of angiogenesis and fibroblast function. *Theranostics* 2018;**8**:169−84.
35. Hu Y, Zhang Y, Ni CY, Chen CY, Rao SS, Yin H, et al. Human umbilical cord mesenchymal stromal cells-derived extracellular vesicles exert potent bone protective effects by CLEC11A-mediated regulation of bone metabolism. *Theranostics* 2020;**10**:2293−308.
36. Manning CE, Eagle AL, Kwiatkowski CC, Achargui R, Woodworth H, Potter E, et al. Hippocampal subgranular zone FosB expression is critical for neurogenesis and learning. *Neuroscience* 2019;**406**:225−33.
37. Liu N, Matsumura H, Kato T, Ichinose S, Takada A, Namiki T, et al. Stem cell competition orchestrates skin homeostasis and ageing. *Nature* 2019;**568**:344−50.
38. Freitas-Rodríguez S, Folgueras AR, López-Otín C. The role of matrix metalloproteinases in aging: tissue remodeling and beyond. *Biochim Biophys Acta Mol Cell Res* 2017;**1864**:2015−25.
39. Gabasa M, Radisky ES, Ikemori R, Bertolini G, Arshakyan M, Hockla A, et al. MMP1 drives tumor progression in large cell carcinoma of the lung through fibroblast senescence. *Cancer Lett* 2021;**507**:1−12.
40. Collado M, Medema RH, Garcia-Cao I, Dubuisson ML, Barradas M, Glassford J, et al. Inhibition of the phosphoinositide 3-kinase pathway induces a senescence-like arrest mediated by $p27^{Kip1}$. *J Biol Chem* 2000;**275**:21960−8.
41. Kennedy AL, Adams PD, Morton JP. Ras, PI3K/Akt and senescence: paradoxes provide clues for pancreatic cancer therapy. *Small GTPases* 2011;**2**:264−7.
42. Kortlever RM, Bernards R. Senescence, wound healing and cancer: the PAI-1 connection. *Cell Cycle* 2006;**5**:2697−703.
43. Guo LJ, Luo XH, Xie H, Zhou HD, Yuan LQ, Wang M, et al. Tissue inhibitor of matrix metalloproteinase-1 suppresses apoptosis of mouse bone marrow stromal cell line MBA-1. *Calcif Tissue Int* 2006;**78**:285−92.
44. de Magalhães JP, Stevens M, Thornton D. The business of anti-aging science. *Trends Biotechnol* 2017;**35**:1062−73.

45. Wong GC, Chow KH. DNA damage response-associated cell cycle re-entry and neuronal senescence in brain aging and Alzheimer's disease. *J Alzheimers Dis* 2023;**94**:S429−51.
46. Sikora E, Bielak-Zmijewska A, Dudkowska M, Krzystyniak A, Mosieniak G, Wesierska M, et al. Cellular senescence in brain aging. *Front Aging Neurosci* 2021;**13**:646924.
47. Xiao Y, Cai GP, Feng X, Li YJ, Guo WH, Guo Q, et al. Splicing factor YBX1 regulates bone marrow stromal cell fate during aging. *EMBO J* 2023;**42**:e111762.
48. Tang X, Li PH, Chen HZ. Cardiomyocyte senescence and cellular communications within myocardial microenvironments. *Front Endocrinol* 2020;**11**:280.
49. Shigdar S, Staunton C, Vasilaki A, McArdle A. Senescence in myoblasts; role in age-related muscle dysfunction. *FASEB J* 2018;**32**: 907.2.
50. Wlaschek M, Maity P, Makrantonaki E, Scharffetter-Kochanek K. Connective tissue and fibroblast senescence in skin aging. *J Invest Dermatol* 2021;**141**:985−92.
51. Lähteenvuo J, Rosenzweig A. Effects of aging on angiogenesis. *Circ Res* 2012;**110**:1252−64.
52. Ambrose C. Muscle weakness during aging: a deficiency state involving declining angiogenesis. *Ageing Res Rev* 2015;**23**:139−53.
53. Kusumbe AP, Ramasamy SK, Adams RH. Coupling of angiogenesis and osteogenesis by a specific vessel subtype in bone. *Nature* 2014; **507**:323−8.
54. Vincenza Carriero M, Franco P, Vocca I, Alfano D, Longanesi-Cattani I, Bifulco K, et al. Structure, function and antagonists of urokinase-type plasminogen activator. *Front Biosci* 2009;**14**: 3782−94.
55. Martin-McNulty B, Zhang L, da Cunha V, Vincelette J, Rutledge JC, Vergona R, et al. Urokinase-type plasminogen activator deficiency (uPA-KO) prevented carotid artery ligation-induced vascular remodeling in mice. *Transl Res* 2007;**149**:70−5.
56. Klimovich PS, Semina EV, Karagyaur MN, Rysenkova KD, Sysoeva VY, Mironov NA, et al. Urokinase receptor regulates nerve regeneration through its interaction with $\alpha 5\beta 1$-integrin. *Biomed Pharmacother* 2020;**125**:110008.
57. Heymans S, Pauschinger M, De Palma A, Kallwellis-Opara A, Rutschow S, Swinnen M, et al. Inhibition of urokinase-type plasminogen activator or matrix metalloproteinases prevents cardiac injury and dysfunction during viral myocarditis. *Circulation* 2006;**114**:565−73.
58. Levy E, Kornowski R, Gavrieli R, Fratty I, Greenberg G, Waldman M, et al. Long-lived αMUPA mice show attenuation of cardiac aging and leptin-dependent cardioprotection. *PLoS One* 2015;**10**:e0144593.
59. Yanai H, Toren D, Vierlinger K, Hofner M, Nöhammer C, Chilosi M, et al. Wound healing and longevity: lessons from long-lived αMUPA mice. *Aging* 2015;**7**:167−76.
60. Zhao L, Giannou AD, Xu Y, Shiri AM, Liebold I, Steglich B, et al. Efferocytosis fuels malignant pleural effusion through TIMP1. *Sci Adv* 2021;**7**:eabd6734.
61. Cabral-Pacheco GA, Garza-Veloz I, Castruita-De la Rosa C, Ramirez-Acuña JM, Perez-Romero BA, Guerrero-Rodriguez JF, et al. The Roles of matrix metalloproteinases and their inhibitors in human diseases. *Int J Mol Sci* 2020;**21**:9739.
62. Dong J, Ma Q. TIMP1 promotes multi-walled carbon nanotube-induced lung fibrosis by stimulating fibroblast activation and proliferation. *Nanotoxicology* 2017;**11**:41−51.
63. Geoffroy V, Marty-Morieux C, Le Goupil N, Clement-Lacroix P, Terraz C, Frain M, et al. *In vivo* inhibition of osteoblastic metalloproteinases leads to increased trabecular bone mass. *J Bone Miner Res* 2004;**19**:811−22.
64. Yokose U, Hachiya A, Sriwiriyanont P, Fujimura T, Visscher MO, Kitzmiller WJ, et al. The endogenous protease inhibitor TIMP-1 mediates protection and recovery from cutaneous photodamage. *J Invest Dermatol* 2012;**132**:2800−9.